

# Constraining a spin 1 dark matter model through CMB observations

An investigation of the additional constraints set from energy injection in the early Universe to relic density constraints

Master's thesis in Physics

Alex Bökmark

Department of Physics

CHALMERS UNIVERSITY OF TECHNOLOGY  
Gothenburg, Sweden 2021  
[www.chalmers.se](http://www.chalmers.se)



MASTER'S THESIS 2021

# Constraining a spin 1 dark matter model through CMB observations

An investigation of the additional constraints set from energy injection in the early Universe to relic density constraints

ALEX BÖKMARK



Department of Physics  
*Division of Subatomic, High Energy and Plasma Physics*  
CHALMERS UNIVERSITY OF TECHNOLOGY  
Gothenburg, Sweden 2021

Constraining a spin 1 dark matter model through CMB observations  
An investigation of the additional constraints set from energy injection in the early  
Universe to relic density constraints  
ALEX BÖKMARK

© ALEX BÖKMARK, 2021.

Supervisor: Riccardo Catena, Associate Professor, Subatomic, High Energy and  
Plasma Physics  
Examiner: Ulf Gran, Professor, Subatomic, High Energy and Plasma Physics

Master's Thesis 2021  
Department of Physics  
Division of Subatomic, High Energy and Plasma Physics  
Chalmers University of Technology  
SE-412 96 Gothenburg  
Telephone +46 31 772 1000

Typeset in L<sup>A</sup>T<sub>E</sub>X  
Printed by Chalmers Reproservice  
Gothenburg, Sweden 2021



# Abstract

During the last century, overwhelming evidence has been presented to infer the existence of additional mass in the Universe, not accounted for by the observable matter content. This unknown form of matter has come to be known as Dark Matter (DM), and the leading hypothesis is that it mainly consists of new, yet-to-be discovered particles. There are different methods of probing DM, one of which is to study how annihilating DM particles would have injected energy in the early Universe and altered the appearance of the Cosmic Microwave Background (CMB) power spectrum, an approach previously used to set constraints on generic DM models. In this thesis, I investigate the prospects for using this approach to constrain certain DM model parameters.

Considering a specific spin 1 DM model, the impact of its annihilation on the CMB power spectrum was investigated by implementing the model Lagrangian in GAMBIT, from which the annihilation cross section was evaluated, and used to determine the energy injected in the early Universe and how the power spectrum would have been affected. Comparing with CMB data, the likelihood for the specific set of parameter values was evaluated and then used to further sample the parameter space, allowing statistical exclusion limits to be set. Combining this with additional constraints, set from the observed DM relic density, it was possible to exclude large regions in the parameter space for the investigated model and set stringent limits on the corresponding DM mass,  $m_\chi \in (\sim 10^2, \sim 10^3)$  GeV, for the specific cases considered. It was thus found that the CMB power spectrum can be used to constrain model parameters, and used in combination with relic density constraints to exclude large regions in the parameter space.

Not only can these results be used in future research when considering the same model, but this thesis provides a practical example of how to implement and use GAMBIT to set constraints on model parameters from observational data, which can also be incorporated for new models in future research.

Keywords: dark matter, annihilating, CMB, relic density, GAMBIT, constraints.



# Acknowledgements

I would like to thank my supervisor Riccardo Catena for sparking my interest for the field of dark matter in the first place and for aiding me through this thesis project. I would also like to thank Emil Åstrand who has helped keep me sane despite the many obstacles and issues encountered and provided valuable assistance towards the completion of this thesis. Finally I extend a thank you to my other friends that have made this pandemic-infested time endurable.

Alex Bökmark, Gothenburg, June 2021



# Contents

<b>1</b>	<b>Introduction</b>	<b>1</b>
1.1	Purpose . . . . .	2
1.2	Thesis outline . . . . .	2
<b>2</b>	<b>Background</b>	<b>3</b>
2.1	Evidence for dark matter . . . . .	3
2.1.1	Galaxy rotation curves . . . . .	3
2.1.2	Gravitational lensing . . . . .	4
2.1.3	Cosmic microwave background . . . . .	4
2.2	Dark matter searches . . . . .	5
2.2.1	Direct detection . . . . .	6
2.2.2	Indirect detection . . . . .	6
2.2.3	Constraints . . . . .	6
<b>3</b>	<b>Theoretical framework</b>	<b>9</b>
3.1	Dark matter models . . . . .	9
3.1.1	Standard model portals . . . . .	9
3.1.2	Beyond standard model portals . . . . .	10
3.2	Impact of annihilating dark matter . . . . .	13
3.2.1	Cross section . . . . .	13
3.2.2	Energy injection . . . . .	14
3.2.3	Relic density . . . . .	16
<b>4</b>	<b>Method</b>	<b>17</b>
4.1	Numerics . . . . .	17
4.1.1	Likelihood computation . . . . .	17
4.1.2	Sampling . . . . .	19
4.2	Practical implementation . . . . .	21
4.2.1	Setting up GAMBIT . . . . .	21
4.2.2	Additional files in GAMBIT . . . . .	25
4.2.3	Additional files in the micrOMEGAs backend . . . . .	27
4.2.4	Implementing the Lagrangian . . . . .	28
4.2.5	Executing the program . . . . .	28
4.3	Obstacles . . . . .	29
4.3.1	Practical implementation . . . . .	29
4.3.2	Parameter space . . . . .	29

4.3.2.1	Sampling . . . . .	29
4.3.2.2	Limits . . . . .	29
<b>5</b>	<b>Results</b>	<b>31</b>
5.1	Relic density . . . . .	31
5.1.1	Validation . . . . .	31
5.1.2	Parameter constraints . . . . .	33
5.2	Cosmic microwave background . . . . .	36
5.2.1	Validation . . . . .	36
5.2.2	Parameter constraints . . . . .	39
5.3	Combined constraints . . . . .	41
5.4	Confidence interval . . . . .	42
<b>6</b>	<b>Discussion</b>	<b>43</b>
6.1	Uncertainties . . . . .	44
6.2	Further development . . . . .	45
<b>7</b>	<b>Conclusions</b>	<b>47</b>
	<b>Bibliography</b>	<b>49</b>
<b>A</b>	<b>Implementation</b>	<b>I</b>
A.1	Modifying GAMBIT . . . . .	I
A.1.1	Defining the model <code>AnnihilatingDM_Thesis</code> . . . . .	I
A.1.2	Defining the local function <code>CalculateSigmaV</code> . . . . .	I
A.1.3	Declaring the model <code>AnnihilatingDM_Thesis</code> . . . . .	IV
A.1.4	Defining the function <code>energy_injection</code> ... . . . .	IV
A.1.5	Declaring the function <code>energy_injection</code> ... . . . .	V
A.1.6	Defining the functions <code>RD_oh2_Thesis</code> and <code>CalculateOmega</code> . . . . .	V
A.1.7	Declaring the function <code>RD_oh2_Thesis</code> . . . . .	VIII
A.1.8	Additional functions to save parameters . . . . .	VIII
A.1.9	Declaring parameter functions . . . . .	IX
A.2	Modifying micrOMEGAs . . . . .	IX
A.2.1	Calculating the relic density . . . . .	IX
A.2.2	Calculating the cross section . . . . .	X
A.3	Implementing the Lagrangian . . . . .	XII
A.3.1	Model file . . . . .	XII
A.3.2	Expanding the Lagrangian . . . . .	XIV
A.4	Executing the model . . . . .	XIV
A.4.1	YAML file for cosmic microwave background constraints . . . . .	XIV
A.4.2	YAML file for relic density constraints . . . . .	XVII
<b>B</b>	<b>Additional figures</b>	<b>XIX</b>
B.1	Relic density . . . . .	XIX
B.2	Cosmic microwave background . . . . .	XXI
B.3	Combined constraints . . . . .	XXV

# 1

## Introduction

Throughout recent centuries, astronomers have speculated of some unknown content in the Universe when trying to describe the dynamics of celestial bodies, seeing it could not be explained by the gravitational influence of the visible matter content alone [1]. This unknown content was for a long time believed to consist of faint stars and other objects known to exist. Being undetectable, this content became referred to as "dark" and is to this day referred to as Dark Matter (DM). Today it is widely accepted that the majority of matter in the Universe is dark. The evidence for its existence is overwhelming, coming from various cosmological phenomena such as galactic rotation curves, gravitational lensing and the Cosmic Microwave Background (CMB) radiation, to name a few. Despite the evidence of its existence, the nature of DM is completely unknown, with the leading hypothesis being that it consists of new species of particles that lie beyond the Standard Model (SM) of particle physics. Despite being extensively sought after experimentally, DM has not yet been detected and remains one of, if not the greatest mystery in modern day science.

With the particle nature of DM being unknown, present approaches to study and probe DM include creating hypothetical models describing its particle nature. With the particle nature being assumed, the impact it would have on certain cosmological parameters can be studied. In particular, if the DM particle annihilates or decays to SM particles, it would have altered the energy content in the early Universe. This energy injection would have affected the ionisation history of the early Universe, which would have altered the appearance of the CMB power spectrum [2]. How the CMB power spectrum would have been affected can be derived theoretically from the assumed DM model, and this needs to be in agreement with the observed one. Thus, studying a DM model with annihilating or decaying DM, the model parameter values must be such that the derived CMB power spectrum is in agreement with the observed one, and can thus be constrained.

In this thesis, the prospects for using the above mentioned approach to constrain DM models has been investigated by considering a specific spin 1 DM model with annihilating DM, interacting with SM particles through a spin 0 mediator, and attempting to constrain its parameter values.

### 1.1 Purpose

The main purpose of this thesis is to investigate the prospects for studying the effects of energy injection from annihilating DM in the early Universe on the CMB power spectrum to set constraints on DM models. Specifically, the case of vectorial (spin 1) DM annihilating to electron-positron pairs via a scalar (spin 0) mediator state has been investigated, with the aim to set constraints on the model parameters for this scenario. Is studying the effects of energy injection from annihilating DM in the early Universe a viable approach to constrain DM model parameters, and what constraints can be inferred on the above mentioned DM model?

### 1.2 Thesis outline

This thesis begins with a background, chapter 2, where several pieces of evidence for the existence of DM are first presented, after which two methods to search for DM are discussed. The theoretical framework within which this thesis has been performed is then presented in chapter 3, first giving some background and motivation for the specific DM model considered and then discussing the implications annihilating DM would have had that may be observed today. In chapter 4, a detailed description of the methodology behind the results is presented. The obtained results are provided in chapter 5, to be discussed in chapter 6 and finally, in chapter 7, conclusions that may be drawn from this thesis and its results are presented. In addition, the practical implementation of the code used to yield the presented results has been carefully documented and is presented in appendix A.



# 2

## Background

It has been firmly established that most of the matter content in the Universe is made up of DM [1], and one of the greatest challenges in science today is to observe it. In this chapter some of the evidence for DM is first discussed in section 2.1, after which some experimental procedures that aim to detect it are discussed in section 2.2.

### 2.1 Evidence for dark matter

The existence of additional matter in the Universe, other than what we are able to see, has been known for almost a century. One of the earliest pieces of evidence for this additional matter came from Fritz Zwicky in 1933, who used the Virial Theorem to estimate the total amount of matter density in the Coma galaxy cluster, which was in disagreement with the amount of visible stellar populations [3]. This additional matter was initially believed to be in the form of stars and gas, undetectable by instruments at the time. Since then, evidence for DM has been presented from many other sources. In this section, some pieces of evidence for the existence of DM are described.

#### 2.1.1 Galaxy rotation curves

The dynamics of planetary bodies is well explained by Keplers laws. In particular, Keplers third law states that "the square of the time taken by any planet to make a complete orbit is proportional to the cube of its mean distance from the Sun" [4]. If the orbit is close to circular, the orbital velocity,  $v$ , can be considered constant throughout the orbit and the orbital period can be expressed as  $T \sim 2\pi \frac{R}{v}$ , with  $R$  being the radius of the orbit. Keplers third law thus states that

$$\left(\frac{R}{v}\right)^2 \propto R^3 \Rightarrow v \propto \frac{1}{\sqrt{R}}, \quad (2.1)$$

meaning the orbital velocity decreases with distance to the massive object.

Studying a spiral galaxy, it is clear that the visible matter is concentrated in the centre of the galaxy. Objects at the outskirts of the galaxy were therefore assumed to obey Keplerian motion, as the system dynamics resembles that of planetary motion. As such the orbital velocity was believed to decrease for increased radii from the galactic centre, just as for planetary motion. However, when measuring the orbital

velocity of objects in the Galaxy, summarised in so called rotation curves, they were found to remain constant for large radii [1]. This contradicted the notion that the majority of mass in galaxies is concentrated in their centre. A possible explanation for this discrepancy was presented by stating that galaxies are engulfed in large spherical "halos" of matter which can not be detected by current instruments, i.e., DM [1]. This can be explained as follows. For an object orbiting some massive source, at distance  $R$ , the orbital velocity,  $v(R)$ , can be expressed in terms of the inward acceleration,  $a(R)$ , which is further dependent on the gravitational potential from the source,  $V(R)$ . This relationship can be expressed as

$$\frac{v^2(R)}{R} = a(R) = \frac{\partial V(R)}{\partial R}, \quad V(R) = -\frac{GM(R)}{R}, \quad (2.2)$$

where  $G$  is the gravitational constant and  $M(R)$  is the enclosed mass within a sphere of radius  $R$ . If the visible matter content constitutes all of the matter, the enclosed matter will be constant,  $M^*$ , at sufficiently large radii. The rotational velocity could then be expressed as

$$v(R) = \sqrt{R \frac{\partial}{\partial R} \left[ -\frac{GM^*}{R} \right]} = \sqrt{RGM^* \frac{1}{R^2}} \propto \frac{1}{\sqrt{R}}, \quad (2.3)$$

as expected from standard Keplerian motion. If, on the other hand, there exist additional mass with some radial density distribution,  $\rho(R)$ , the enclosed mass would, for sufficiently large radii, instead be expressed as

$$M(R) = M^* + 4\pi \int_0^R \rho(R') R'^2 dR'. \quad (2.4)$$

Selecting appropriate density distributions, the orbital velocity can be obtained such that it approaches constant values for large radii, explaining the observed rotation curves.

### 2.1.2 Gravitational lensing

A consequence of Einsteins general theory of relativity is that the four-dimensional spacetime we inhabit is curved by matter. Light travelling in a straight line will follow the curvature of spacetime and will subsequently "bend" when passing by massive objects. Massive objects in space can therefore be used as so-called gravitational lenses, which act on passing light and distort or magnify images of sources that lie beyond the lens. When studying e.g. elliptical galaxies, gravitational lensing can be used to determine the distribution of matter. When doing this it has been found that the distribution of matter extends the distribution of visible baryonic matter, suggesting the existence of DM [5].

### 2.1.3 Cosmic microwave background

Shortly after the Big Bang, the Universe was a lot denser and hotter than today. For some time it was too hot to sustain the formation of stable atoms and the Universe

was filled with a hydrogen plasma where photons and baryons were coupled through Thomson scattering [2]. As the Universe expanded and cooled, it eventually became sufficiently cold for protons and electrons to combine to form neutral hydrogen. The hydrogen atoms could not scatter the radiation as the plasma had, and photons could now propagate freely without constantly interacting with the surrounding matter [2]. These photons have propagated freely ever since, constantly growing less energetic as their wavelengths continuously grow larger with the expansion of the Universe. Today this radiation is detected from all directions and corresponds to a thermal black body spectrum at a temperature of  $T_{\text{CMB}} = 2.7255$  K [6] with anisotropies of the order of one part in  $10^5$ . This is the so-called Cosmic Microwave Background (CMB) [7]. The temperature anisotropy can be described as [2]

$$\Theta(\hat{\mathbf{n}}) \equiv \frac{T(\hat{\mathbf{n}}) - T_{\text{CMB}}}{T_{\text{CMB}}} = \sum_{\ell=0}^{\infty} \sum_{m=-\ell}^{\ell} a_{\ell m} Y_{\ell m}(\hat{\mathbf{n}}), \quad (2.5)$$

where  $T(\hat{\mathbf{n}})$  is the temperature field as measured in a given direction  $\hat{\mathbf{n}}$ . As indicated by the second equality, the temperature anisotropy can be described as an infinite sum of the spherical harmonics  $Y_{\ell m}(\hat{\mathbf{n}})$  for a given integer multipole  $\ell \geq 0$  and angular index  $m = -\ell, \dots, \ell$  with weights  $a_{\ell m}$ . The angular power spectrum,  $C_{\ell}$  is defined as the 2-point correlation function of  $a_{\ell m}$ , and the theoretical expectation of the temperature power spectrum can be written as [2]

$$C_{\ell}^{TT} = \frac{1}{2\ell + 1} \sum_m \langle a_{\ell m} a_{\ell m}^* \rangle, \quad (2.6)$$

where  $\langle \rangle$  is the average over many sky realisations<sup>1</sup>. In similar fashion, the power spectra of the polarisation of CMB photons can be obtained which gives additional information about the early Universe [2]. This polarisation can be split into electric (E) and magnetic (B) components. One can also obtain *cross-correlation* spectra such as  $C_{\ell}^{TE}$  which provides additional independent constraints. The positions and sizes of the peaks in the power spectra correspond to theoretical power spectra of a Universe with flat geometry, 5% baryonic matter and 27% DM [8], providing quantitative evidence for the existence of DM.

## 2.2 Dark matter searches

With the existence of DM being strongly supported by current observations, it is of great interest to observe and describe its particle nature. Despite being extensively sought after, the particles forming DM are yet to be detected. In this section, two methods used in the search for DM are briefly discussed.

<sup>1</sup>The initial value of all cosmic fields (e.g. density and pressure of the energy components in our Universe) is unknown. It is typically modelled as a stochastic variable obeying a Gaussian probability density function (pdf). Each choice of initial conditions corresponds to a different realisation of our Cosmos (i.e. of the observed sky). Cosmological observables are then defined as averages over over such a pdf, i.e. over different realisations of the observed sky.

### 2.2.1 Direct detection

A consequence of our galaxy being embedded in a DM halo is that we are bombarded with DM particles. This enables attempts for so-called direct detection, i.e., observing DM particles directly interacting with SM particles. Observing such interactions would allow for specific descriptions of the particle nature of the DM particles being formulated. When trying to observe such interactions one seeks to measure the nuclear recoil caused by the scattering of a DM particle and several past experiments have attempted to do this, e.g., [9]-[14]. At such direct detection experiments the scattering rate of DM particles will be very low and other sources of scattering will be present, it is therefore essential to be able to discriminate the DM signals from such background signals. Furthermore, what determines the sensitivity to DM signals for a certain experiment will be a combination of the energy threshold, control of the background and exposure as well as the target for the experiment [15]. Past direct detection experiments have not been able to detect scattering rate significantly over the background. These null results can however be used to set limit on the DM particles, which will be discussed in section 2.2.3.

### 2.2.2 Indirect detection

As opposed to direct detection, indirect detection relies on detecting byproducts of DM annihilation or decay over the expected background [15]. The specific experimental setup relies on the final product of either the annihilation or the decay. Focusing on annihilating DM, one common example is studying gamma-rays as the final product. The gamma-ray flux produced from DM annihilation should be proportional to the number density squared of particles, the DM annihilation cross section, the mean DM velocity, the volume of sky observed and the energy spectrum [15]. One important aspect of indirect DM detection is that the annihilation cross section can be velocity-independent, and the bounds on the annihilation cross section is then directly related to the DM relic density [15].

One approach for indirect detection has been to study celestial bodies such as neutron stars or brown dwarfs at which the DM particles should accumulate and thus increase the rate of DM annihilation in these regions [16]. If the final states of the annihilation process is sufficiently long-lived to escape it could then subsequently decay to observable radiation [16]. Such approaches have been investigated, [16, 17], but no detection has yet been made.

### 2.2.3 Constraints

Despite not having detected DM, the null results of the direct detection experiments along with the indirect detection experiments have been used to set constraints on the particle nature of DM in the form of excluded regions in certain parameter spaces. One of the most interesting and general parameter describing the particle nature of DM is its mass. Despite not being able to restrict the DM particle mass as a single parameter, parameter spaces such as the DM mass - cross section have been

constrained, predominantly from the null results of direct detection experiments [15].

## 2. Background

---

# 3

## Theoretical framework

In this thesis, parameters related to a specific DM model have been constrained by comparing the model predictions to CMB observations. This chapter is devoted to explain the theoretical framework used to perform this comparison. In section 3.1 the investigated DM model is motivated and described and in section 3.2 the effects of the DM model, used to constrain the model, are described.

### 3.1 Dark matter models

Despite overwhelming amount of evidence supporting the existence of DM, as mentioned in section 2.1, its nature is still unknown. In order for detection of the DM particle to be possible, it must interact with SM particles in some way, albeit weakly - if it does not, it will not be possible to detect the particle directly. To obtain a model to investigate, certain aspects of the DM particle nature must be assumed. In this thesis it is assumed that the DM particle is vectorial, i.e., has spin 1. The possibility that the DM particle directly interacts with SM fermions is strongly disfavoured by experiments [15], and it is therefore further assumed that the DM particle interacts with a mediator particle, which in turn interacts with SM fermions, a scenario often referred to as portal. There are two distinct possibilities for such portal, it will either be a known SM particle that accounts for the mediator state or it will be a new particle which lies Beyond the Standard Model (BSM) of particle physics. The possibility of these two cases will be discussed in section 3.1.1 and section 3.1.2 respectively.

#### 3.1.1 Standard model portals

Models with SM portals include DM models where the DM state interacts with the SM states through either the Higgs boson or the Z boson. Assuming the vectorial DM particle is a pure SM singlet, i.e. neutral under the SM gauge groups, it is possible to construct a four-field operator connecting the DM bilinear to the Higgs bilinear as [15]

$$\frac{1}{2}\lambda_{\chi H}\chi^\mu\chi_\mu H^\dagger H, \quad (3.1)$$

where  $\lambda_{\chi H}$  is the coupling strength between the DM particle and the Higgs boson,  $\chi^\mu$  is the vectorial DM field and  $H = \begin{pmatrix} 0 \\ \frac{v_h+h}{\sqrt{2}} \end{pmatrix}$ , where  $v_h$  is the Vacuum Expectation Value (VEV) and  $h$  is the physical SM Higgs boson. Note that an addition

to the SM model Lagrangian in this way would be invariant under a  $\mathbb{Z}_2$  symmetry where  $\chi^\mu \rightarrow -\chi^\mu$ . This extension to the SM model has been investigated and largely excluded from direct detection experiments, as well as collider experiments investigating the branching ratio of invisible mass from annihilating/decaying Higgs bosons [15].

Constructing a similar connection between the DM and SM states through the Z boson is not quite as straight-forward, as there is no gauge-invariant way to construct a four-field operator [15]. Instead the connection may be constructed through a 6-dimensional operator, which has also been investigated and thoroughly excluded from direct detection experiments [15].

As the above mentioned portals have been largely disfavoured by experiments, it is in this thesis assumed that the interaction between the DM and SM states occur through a new mediator state, as explained in section 3.1.2.

#### 3.1.2 Beyond standard model portals

In this thesis it is assumed that the mediator state connecting DM and SM particles is a new, yet-to-be discovered scalar field, i.e., has spin 0. The construction of such a theory can be performed by assuming the SM should be extended to include a new  $U_\chi(1)$  gauge group with a single real, charged scalar  $\phi$ . This charged scalar will come to play the role of the mediator field and the SM fermions are assumed to have some (small) charge under this new gauge group; were they entirely neutral under this new gauge group they would not be able to interact with the mediator state and such vertex would imply charge violation. The SM Lagrangian should then be extended to contain the charged scalar and its interactions with both SM particles and the new gauge field,  $\chi_\mu$ , which will play the role of vector DM. The Lagrangian for the hidden sector, containing the interactions of the new fields, can be expressed as [18]

$$\mathcal{L}_{\text{hidden}} = -\frac{1}{4}\tilde{F}_{\mu\nu}\tilde{F}^{\mu\nu} + (D_\mu\phi)^\dagger D^\mu\phi - V(\phi), \quad (3.2)$$

where  $\tilde{F}_{\mu\nu}$  is the field strength tensor of the gauge field  $\chi_\mu$  [19]

$$\tilde{F}_{\mu\nu} = \partial_\mu\chi_\nu - \partial_\nu\chi_\mu, \quad (3.3)$$

$D_\mu$  is the gauge covariant derivative [19]

$$D_\mu\phi = \partial_\mu\phi - i\lambda_\chi\chi_\mu\phi \quad (3.4)$$

and  $V(\phi)$  is the scalar potential, which in analogy with the SM Higgs potential [20] is assumed to be

$$V(\phi) = 2\lambda_S^2 \left(\phi^\dagger\phi - \mu\right)^2, \quad (3.5)$$

where the coupling has been assigned to  $2\lambda_S^2$  for convenience later on. At the minimum of the scalar potential a VEV is obtained as  $\langle\phi\rangle = \frac{v_S}{\sqrt{2}}$ , where  $v_S = \sqrt{2}\mu$ . The scalar field can be expressed as



$$\phi = \frac{S + v_S}{\sqrt{2}}, \quad (3.6)$$

where  $S$  is the physical field around the VEV [20], interpreted as the physical mediator state. Ignoring the first term in the above Lagrangian, as this is purely in the dark sector, the Lagrangian can be expressed as

$$\mathcal{L}_{\text{hidden}} \supset (D_\mu \phi)^\dagger D^\mu \phi - V(\phi) = \left[ \partial_\mu \phi^\dagger + i\lambda_\chi \chi_\mu \phi^\dagger \right] \left[ \partial^\mu \phi - i\lambda_\chi \chi^\mu \phi \right] - 2\lambda_S^2 \left( \phi^\dagger \phi - \mu \right)^2. \quad (3.7)$$

Inserting the scalar field as expressed in eq. (3.6), the first term can be written as

$$\begin{aligned} & \frac{1}{2} \left[ \partial_\mu S + i\lambda_\chi \chi_\mu S + i\lambda_\chi v_S \chi_\mu \right] \left[ \partial^\mu S - i\lambda_\chi \chi^\mu S - i\lambda_\chi v_S \chi^\mu \right] = \\ & = \frac{1}{2} \left[ \partial_\mu S \partial^\mu S - i\lambda_\chi \partial_\mu S \chi^\mu S - i\lambda_\chi v_S \partial_\mu S \chi^\mu + \right. \\ & \quad + i\lambda_\chi \chi_\mu S \partial^\mu S + \lambda_\chi^2 \chi_\mu \chi^\mu S S + \lambda_\chi^2 v_S \chi_\mu \chi^\mu S + \\ & \quad \left. + i\lambda_\chi v_S \chi_\mu \partial^\mu S + \lambda_\chi^2 v_S \chi_\mu \chi^\mu S + \lambda_\chi^2 v_S^2 \chi_\mu \chi^\mu \right] = \\ & = \frac{1}{2} \partial_\mu S \partial^\mu S + \frac{1}{2} \lambda_\chi^2 \chi_\mu \chi^\mu S S + \lambda_\chi^2 v_S \chi_\mu \chi^\mu S + \frac{1}{2} \lambda_\chi^2 v_S^2 \chi_\mu \chi^\mu. \end{aligned} \quad (3.8)$$

Ignoring the first term, which does not contribute to the interaction, and inserting the scalar field as expressed in eq. (3.6) in the second term in eq. (3.7), the Lagrangian can further be rewritten as

$$\mathcal{L}_{\text{hidden}} \supset \frac{1}{2} \lambda_\chi^2 \chi_\mu \chi^\mu S S + \lambda_\chi^2 v_S \chi_\mu \chi^\mu S + \frac{1}{2} \lambda_\chi^2 v_S^2 \chi_\mu \chi^\mu - \frac{\lambda_S^2}{2} S S S S - 2\lambda_S^2 v_S S S S - 2\lambda_S^2 v_S^2 S S. \quad (3.9)$$

From the third and final terms the masses of  $\chi_\mu$  and  $S$  can be read off to be  $m_\chi = \lambda_\chi v_S$  and  $m_S = 2\lambda_S v_S$  respectively. Neglecting the mass terms and the quartic self-interaction of  $S$ , which do not contribute to the coupling between the fields, the Lagrangian can be further rewritten as

$$\mathcal{L}_{\text{hidden}} \supset \lambda_\chi m_\chi \chi_\mu \chi^\mu S + \frac{1}{2} \lambda_\chi^2 \chi_\mu \chi^\mu S S - \lambda_S m_S S S S. \quad (3.10)$$

Compensating for implicit summation of terms with interchanged positions of fields, the total contribution to the Lagrangian for the interaction between  $\chi_\mu$  and  $S$  can be expressed as

$$\mathcal{L}_{\chi S} = \frac{1}{2} \lambda_\chi m_\chi \chi_\mu \chi^\mu S + \frac{1}{8} \lambda_\chi^2 \chi_\mu \chi^\mu S S - \frac{\lambda_S m_S}{3!} S S S. \quad (3.11)$$

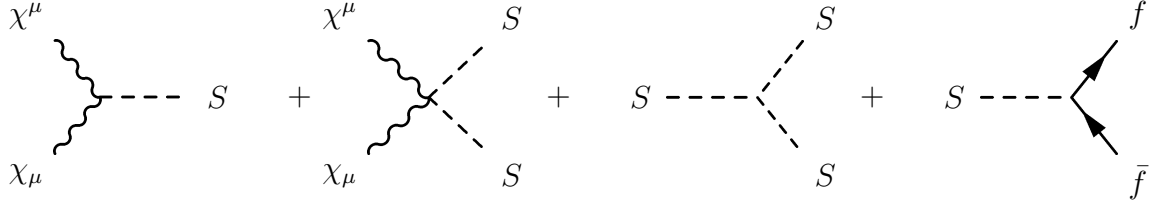
The interaction between the mediator state and the fermionic SM states is assumed to resemble the Higgs interaction [15];

$$\mathcal{L}_{\text{portal}} = \frac{\lambda_{Sf} m_f}{\sqrt{2} v_h} S \bar{f} f, \quad (3.12)$$

where the couplings  $\lambda_{Sf}$  are dependent on the SM fermion charge under the new gauge group. Adding the above contributions, the investigated Lagrangian is

$$\mathcal{L}_{\text{DM}} = \mathcal{L}_{\chi S} + \mathcal{L}_{\text{portal}} = \frac{1}{2} \lambda_{\chi} m_{\chi} \chi_{\mu} \chi^{\mu} S + \frac{1}{8} \lambda_{\chi}^2 \chi_{\mu} \chi^{\mu} S S + \frac{\lambda_{Sf} m_f}{\sqrt{2} v_h} S \bar{f} f - \frac{\lambda_S m_S}{3!} S^3. \quad (3.13)$$

This specific extension to the SM is one of many possible ways to incorporate new, unknown particles. In this thesis the model considered is the one described in eq. (3.13) and the aim has been to set constraints on the model parameters  $m_{\chi}$ ,  $m_S$ ,  $\lambda_{\chi}$ ,  $\lambda_{Sf}$  and  $\lambda_S$ . When comparing to CMB data, the only SM fermion final state considered is  $e^+ e^-$ . For illustrative purposes, the relevant Feynman diagrams are depicted below.



## 3.2 Impact of annihilating dark matter

This section is dedicated to describe how the DM annihilation would have affected the CMB power spectrum and the DM relic density. As the cross section is of great importance to derive how the power spectrum and relic density are affected, a brief discussion regarding the cross section is first presented in section 3.2.1. How the annihilating DM would have injected energy in the early Universe and affected the power spectrum is then described in section 3.2.2 and finally how the relic density would have been affected is described in section 3.2.3.

### 3.2.1 Cross section

When interested in specific processes within particle physics it is common practice to discuss the cross section of the process. This is in some way analogous to the probability of that process occurring; larger cross section for a specific process implies larger chance of that process occurring. Given a specific model, i.e., specific Lagrangian, the differential cross section for  $2 \rightarrow 2$  interactions can be expressed in the centre of mass frame as [21]

$$\frac{d\sigma}{d\Omega} = \frac{1}{4|E_1\vec{p}_2 - E_2\vec{p}_1|} \frac{|\vec{q}_1|}{16\pi^2\sqrt{s}} |\mathcal{M}|^2, \quad (3.14)$$

where  $\vec{p}_i$  and  $E_i$  are the momentum and energy for incoming particle  $i$ ,  $\vec{q}_i$  is the momentum for the outgoing particle  $i$ ,  $s$  is the Mandelstam variable  $s = (p_1 + p_2)^2$ ,  $d\Omega$  is the spherical angle element of the direction of the outgoing particle 1, corresponding to  $\vec{q}_1$ , and  $|\mathcal{M}|^2$  is the appropriate matrix element. The matrix element can be derived from the Lagrangian and the Feynman rules, in this thesis this is performed by FeynRules [22]. The total cross section is then obtained by integrating over  $d\Omega$ . Since the total cross section is connected to a specific particle interaction, i.e., dependent on the momentum of the particles in question for that specific interaction, it is more convenient to use the thermally averaged cross section, which can be viewed as an average of the cross section over a non-relativistic classic gas, i.e., for many such interactions with reasonably low velocities. The thermally averaged annihilation cross section can be calculated numerically as [23]

$$\langle\sigma v\rangle = \frac{\sum_{i,j} g_i g_j \int_{(m_i+m_j)^2} ds \sqrt{s} K_1(\sqrt{s}/T) p_{ij}^2 \sigma_{ij}(s)}{2T \left( \sum_i g_i m_i^2 K_2(m_i/T) \right)^2}, \quad (3.15)$$

where  $i$  and  $j$  denote the incoming particles,  $g_i$  is the degree of freedom for particle  $i$ ,  $K_n$  is the modified Bessel function of the second kind of order  $n$ ,  $T$  is the temperature at which the interaction occur,  $p_{ij}$  is the momentum of the incoming particles in their centre-of-mass frame;

$$p_{ij} = \frac{1}{2} \left[ \frac{(s - (m_i + m_j)^2)(s - (m_i - m_j)^2)}{s} \right]^{\frac{1}{2}} \quad (3.16)$$

and  $\sigma_{ij}$  is the total annihilation cross section for particles  $i$  and  $j$ , i.e., the combined cross section for annihilation of a DM pair into all of the possible final states;

$$\sigma_{ij} = \sum_{X,Y} \sigma(\chi_i + \chi_j \leftrightarrow X + Y), \quad (3.17)$$

which is evaluated as described above. Note that  $i$  and  $j$  in eq. (3.15) allow for different particle species to be present in the theory, i.e.,  $\chi_1, \chi_2, \dots$ , but for the model eq. (3.13), only one DM particle candidate is present. The thermally averaged cross section has been computed by micrOMEGAs [24].

#### 3.2.2 Energy injection

At the time of recombination DM annihilation will have injected energy into the surrounding medium, the photon-baryon plasma, effectively altering the recombination history. The three main ways the history is altered by the interaction of the particle shower produced by the annihilating DM with the plasma are through ionisation, induced Ly- $\alpha$  excitation of the hydrogen and heating of the plasma [25]. The first two affect the electron fraction  $x_e \equiv n_e/n_H$  while the heating affects the temperature of the intergalactic medium  $T$  [25]. This could lead to distinguishable modifications of the CMB power spectrum [2, 25]. The evolution of these quantities are given by [2]

$$\begin{aligned} \frac{dx_e(z)}{dz} &= \frac{1}{(1+z)H(z)} [R(z) - I(z) - I_\chi(z)], \\ \frac{dT(z)}{dz} &= \frac{1}{1+z} [2T + \gamma(T - T_{\text{CMB}})] - K_h, \end{aligned} \quad (3.18)$$

where  $z$  is the redshift,  $\gamma$  is the Compton scattering rate,  $T_{\text{CMB}}$  is the CMB temperature,  $H(z)$ ,  $I(z)$  and  $R(z)$  are the Hubble constant, ionisation rate and recombination rate at redshift  $z$  and  $K_h$  and  $I_\chi$  are the additional heating and ionisation terms caused by the annihilating DM. The relevant ionisation terms arise from direct ionisation and ionisation from an excited state following excitation and are given as [2]

$$\begin{aligned} I_{\chi,\text{ion}} &= - \frac{1}{n_H E_i} \frac{d^2 E}{dV dt} \bigg|_{\text{dep,ion}}, \\ I_{\chi,\text{exc.}} &= - \frac{1 - \mathcal{C}}{n_H E_\alpha} \frac{d^2 E}{dV dt} \bigg|_{\text{dep,exc.}}, \end{aligned} \quad (3.19)$$

where  $E_i$  is the average ionisation energy per baryon,  $E_\alpha$  is the energy of the Lyman- $\alpha$  transition and  $\mathcal{C}$  is the probability for an excited hydrogen atom to decay before photoionisation can occur (the Peebles C factor). The additional heating term is given as [2]

$$K_h = - \frac{2}{H(z)(1+z)3n_H(1+f_{\text{He}}+x_e)} \frac{d^2 E}{dV dt} \bigg|_{\text{dep,heat}}. \quad (3.20)$$

Note that all terms are proportional to the rate per unit volume that energy is deposited into the surrounding medium via either ionisation, excitation or heating. These rates of energy deposition can be expressed in terms of the rate per unit volume of energy injection through a dimensionless efficiency function as [2]

$$\left. \frac{d^2 E}{dV dt} \right|_{\text{dep}, c}(z, x_e) = f_c(z, x_e) \cdot \left. \frac{d^2 E}{dV dt} \right|_{\text{inj}}(z), \quad (3.21)$$

where  $c$  denotes the channel of energy deposition, i.e., ionisation, excitation or heating. The efficiency function in the case of annihilating DM can be expressed as [2]

$$f_c(z, x_e) = \frac{\sum_{\ell} \int_z^{\infty} d \ln(1+z') \frac{(1+z')^3}{H(z')} \int_0^{E_{\text{max}}} dE T_c^{(\ell)}(z', z, E, x_e) E \left. \frac{d^2 N}{dE dt} \right|_{\text{inj}}^{(\ell)}(z', E)}{\frac{(1+z)^3}{H(z)} \int_0^{E_{\text{max}}} dE E \left. \frac{d^2 N}{dE dt} \right|_{\text{inj}}^{\text{tot}}(z, E)}, \quad (3.22)$$

where  $\left. \frac{d^2 N}{dE dt} \right|_{\text{inj}}^{(\ell)}(z', E)$  is the rate of particle  $\ell$  with energy  $E$  injected at redshift  $z'$ , and  $T_c^{(\ell)}(z', z, E, x_e)$  is the transfer function, which is the probability that a particle  $\ell$ , injected at redshift  $z'$  with energy  $E$  would deposit its remaining energy at redshift  $z$ . For the energy deposition, the particle species of interest are almost exclusively  $\ell \in \{e^{\pm}, \gamma\}$  [2]. The efficiency function is evaluated numerically in CosmoBit [2], and the remaining challenge is to evaluate the rate per unit volume of energy injection, which is given by [2]

$$\left. \frac{d^2 E}{dV dt} \right|_{\text{inj}}(z) = \xi^2(z) \rho_{\text{cdm}}^2 (1+z)^6 \frac{\langle \sigma v \rangle}{m_{\chi}}, \quad (3.23)$$

where  $\xi(z) \equiv \rho_{\chi}(z)/\rho_{\text{cdm}}$  is the fractional abundance of the investigated DM candidate with respect to the abundance of all DM. Note that eq. (3.23) indicates a linear relationship between the rate of energy injection per unit volume and the thermally averaged cross section. In the limit  $\langle \sigma v \rangle \rightarrow 0$  no additional energy will be injected into the primordial plasma, as expected, and the evolutions of  $x_e$  and  $T$  will be identical to the standard evolutions. As the cross section increases, more energy will be injected into the plasma and the evolutions will become more and more distorted. For the model of interest, this indicates that values of parameters will only be restricted to regions where  $\langle \sigma v \rangle$  is sufficiently small, i.e., this method of constraining the parameters will only be able to provide an upper bounds of sorts to the cross section and the parameter values corresponding to these values of the cross section.

In order to calculate the power spectrum  $\{C_{\ell}\}$ , the evaluated efficiency function and the energy spectrum is used as inputs for the module **CLASS** [26]. The power spectrum is then evaluated as [27]

$$C_{\ell}^{XY} = 4\pi \int \frac{dk}{k} \Delta_{\ell}^X(q) \Delta_{\ell}^Y(q) \mathcal{P}(k), \quad (3.24)$$

where  $X$  and  $Y$  denote the evaluated power spectrum, i.e., T or E,  $q$  is the generalised wavenumber

$$q = \sqrt{k^2 + K}, \quad K = -H_0^2(1 - \Omega_{\text{tot}}), \quad (3.25)$$

where  $k$  is the wavenumber,  $H_0$  is the present Hubble expansion rate and  $\Omega_{\text{tot}}$  is the total energy density.  $\mathcal{P}(k)$  is the primordial power spectrum given by [27]

$$\mathcal{P}(k) = A_s k^{n_s-1}, \quad (3.26)$$

where  $A_s$  and  $n_s$  are the amplitude and tilt of the primordial power spectra, specified as input parameters to be  $\ln(10^{10}A_s) = 3.044$  and  $n_s = 0.9649$ . The transfer functions  $\Delta_\ell^X$  encodes the information regarding the injected energy as provided by CosmoBit and are evaluated by CLASS [27].

#### 3.2.3 Relic density

The relic density parameter is defined as [28]

$$\Omega_\chi h^2 \equiv \frac{\rho_\chi}{\rho_c}, \quad (3.27)$$

where  $\rho_\chi$  is the energy density of DM and  $\rho_c = \frac{3H^2}{8\pi G}$  is the critical energy density of the Universe. The observed relic density, according to simulations compared to observed CMB power spectrum, is  $\Omega_\chi h^2 \approx 0.1188$  [29]. The energy density can be evaluated from the number density, using the DM mass as conversion,  $\rho_\chi = m_\chi n_\chi$ . The number density of DM particles, initially in thermal equilibrium with the baryonic plasma at temperature  $T$ , is further described by the Boltzmann equation [30]

$$\frac{dn_\chi}{dt} + 3Hn_\chi = \langle \sigma v \rangle (n_{\chi,\text{eq.}} n_{\bar{\chi},\text{eq.}} - n_\chi n_{\bar{\chi}}), \quad (3.28)$$

where  $H$  is the Hubble rate and

$$n_{\chi,\text{eq.}} = n_{\bar{\chi},\text{eq.}} = \frac{g_\chi m_\chi^2 T K_2\left(\frac{m_\chi}{T}\right)}{2\pi^2}, \quad (3.29)$$

where  $g_\chi$  is the internal degrees of freedom and  $K_2$  is the modified Bessel function of second order. Given a specific model with specified parameter values, such that  $\langle \sigma v \rangle$  can be evaluated as described in 3.2.1 and the DM mass is known, the relic density parameter can be evaluated by solving the Boltzmann equation and compared to the observed value. Doing this one can set constraints on the model parameters. Note that if the investigated DM particle does not constitute all of the DM, the relic density of this particular species would not account for the entirety of the observed relic density. As such, the observed relic density can be considered an upper bound when setting constraints on the model.

# 4

## Method

This chapter is devoted to carefully explaining the methodology behind the obtained results and highlighting certain obstacles encountered. The aim is to allow any reader of this chapter to be able to recreate the results obtained in this thesis and to use this approach as a template for further investigation in this area.

The first section of this chapter provides a description of the numerics used to sample the relevant parameter spaces, section 4.1, after which the full practical implementation of the code is explained in section 4.2 and finally some obstacles and difficulties encountered during this thesis are highlighted in section 4.3.

### 4.1 Numerics

The theoretical predictions of the model eq. (3.13) are compared with data on the CMB angular power spectrum and DM relic density by applying the profile likelihood method [31]. To use the observed relic density and CMB power spectrum to set constraints on the model parameters, the likelihood is evaluated for given sets of model parameter values. How this is done is described in section 4.1.1. By calculating the likelihood of many sampled points in the multidimensional parameter space, the likelihoods are used to select a new set of points in order to maximise the evaluated likelihoods. How this sampling is performed is described in section 4.1.2.

#### 4.1.1 Likelihood computation

When computing the likelihood with respect to the relic density, it is in DarkBit [32] assumed that the likelihood for the correct relic density follows a Gaussian distribution with mean  $\mu_{\text{obs.}} = 0.1188$  and standard deviation  $\sigma_{\text{obs.}} = 0.001$ , in accordance with [23]. Given a specific point in parameter space, a theoretical value of the relic density,  $(\Omega_\chi h^2)_{\text{theory}}$  is obtained as described in section 3.2.3. It is then assumed that the theoretical likelihood also follows a Gaussian distribution with mean  $\mu_{\text{theory}} = (\Omega_\chi h^2)_{\text{theory}}$  and standard deviation  $\sigma_{\text{theory}} = 0.05 \cdot (\Omega_\chi h^2)_{\text{theory}}$ . When performing a scan, the user can choose to scan for regions that obtain the observed relic density, or regions that yield relic densities that are less or equal than the observed relic density. In the first case, a chi-square-like log likelihood is evaluated using the above parameters according to the below expressions [32]

$$\sigma^2 = \sigma_{\text{obs.}}^2 + \sigma_{\text{theory}}^2, \quad (4.1)$$

$$\chi^2 = -\frac{1}{2} \frac{(\mu_{\text{theory}} - \mu_{\text{obs.}})^2}{\sigma^2}, \quad (4.2)$$

$$\log \mathcal{L} = \chi^2 - \frac{1}{2} \log(2\pi\sigma^2). \quad (4.3)$$

If the observed relic density is instead regarded as an upper limit, the log likelihood is evaluated as [32]

$$\sigma^2 = \sigma_{\text{obs.}}^2 + \sigma_{\text{theory}}^2, \quad (4.4)$$

$$\Delta = \mu_{\text{obs.}} - \mu_{\text{theory}} \quad (4.5)$$

$$\log \mathcal{L} = \log \left[ \frac{\exp\left(-\frac{\Delta^2}{2\sigma^2}\right)}{\sigma} \cdot \text{erfc}\left(\frac{\sigma_{\text{obs.}}\Delta}{\sigma_{\text{theory}}\sqrt{2}\sigma}\right) + \frac{\text{erfc}\left(-\frac{\Delta}{\sqrt{2}\sigma_{\text{theory}}}\right)}{\sigma_{\text{obs.}}} \right] - \frac{1}{2} \log[8\pi], \quad (4.6)$$

where  $\text{erfc}$  is the complementary error function

$$\text{erfc}(x) = 1 - \frac{2}{\sqrt{\pi}} \int_0^x e^{-t^2} dt. \quad (4.7)$$

For visualisation, the log likelihoods expressed in eq. (4.3) and eq. (4.6) are plotted as functions of  $(\Omega_\chi h^2)_{\text{theory}}$  in fig. 4.1. When  $\log \mathcal{L}$  has been evaluated for a point in parameter space it is then assigned as the *fitness parameter* for that point, which is used to drive the scan as explained in section 4.1.2.

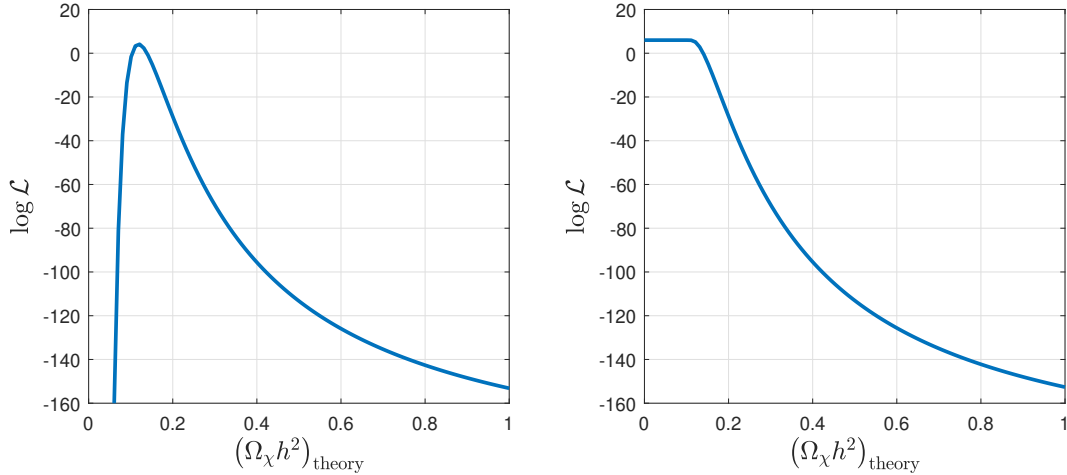


**Figure 4.1:** The log likelihoods as expressed in eq. (4.3) (left) and eq. (4.6) (right) as functions of the theoretical relic density.

Computing the likelihoods related to the CMB power spectra, the GAMBIT backend CosmoBit [2] has been utilised. This backend makes use of the `Planck` likelihood published within the Planck Likelihood Code, `plc` [33], which gives access to the Planck 2018 likelihoods; allowing users to compute the the low- $\ell$  ( $2 \leq \ell \leq 29$ ) and high- $\ell$  ( $30 \leq \ell \leq 2508$ ) log likelihoods for the temperature and polarisation spectra



[2]. In this thesis, three different log likelihoods have been evaluated and these are 1) the log likelihood for the nuisance parameter, 2) the combined log likelihood for TT+EE for low- $\ell$  and 3) the *lite* combined log likelihood for TT+TE+EE for high- $\ell$ . Once these log likelihoods have been evaluated for a certain point in parameter space they are added to form the total log likelihood, to be used as the fitness parameter for this point used to drive the scan as explained in section 4.1.2. Below is a description for the different likelihood calculations.

1) The first likelihood is obtained in the same way as eq. (4.3), but with  $\mu_{\text{theory}} = A_{\text{planck}}$ ,  $\mu_{\text{obs.}} = 1.0$ ,  $\sigma_{\text{obs.}} = 0.1$  and  $\sigma_{\text{theory}} = 0.0$ . The parameter  $A_{\text{planck}}$  encodes the absolute calibration of the observed power spectrum and is a nuisance parameter needed by `plc` [2].

2) The likelihood function in `CosmoBit` evaluates separately the log likelihood for TT and the log likelihood for EE, as provided by `plc`, and then adds them. Both functions require a vector of  $C_{\ell}^{\text{theory}}$  in the range  $\ell \in [0, 29]$ , followed by the Planck calibration nuisance parameter,  $A_{\text{planck}}$ . The power spectrum as described by  $\{C_{\ell}^{\text{theory}}\}$  is obtained as described in section 3.2.2. The likelihood functions then evaluate the approximate solutions [33]

$$\log \mathcal{L}(\mathbf{C}^{\text{theory}} | \mathbf{C}^{\text{data}}) \approx \sum_{\ell=2}^{29} g_{\ell}(C_{\ell}^{\text{data}}, C_{\ell}^{\text{theory}}) + \text{const.}, \quad (4.8)$$

where  $C_{\ell}^{\text{data}}$  and  $g_{\ell}$  are tabulated values and functions, respectively, provided in the `plc` module, derived from the 2018 Planck data [33].

3) The likelihood function provided in `Plik` expects a vector of parameters consisting of the TT CMB power spectrum in the range  $\ell \in [0, 2508]$ , followed by the EE, and TE spectra in the same range and finally followed and by the Planck calibration nuisance parameter,  $A_{\text{planck}}$ . This vector, with total length 7528, may be denoted  $\mathbf{C}(\theta)$ , where  $\theta$  is the parameter vector describing the sampled point. The log likelihood is then evaluated as [33]

$$-\log \mathcal{L}(\hat{\mathbf{C}} | \mathbf{C}(\theta)) = \frac{1}{2} [\hat{\mathbf{C}} - \mathbf{C}(\theta)]^T \Sigma^{-1} [\hat{\mathbf{C}} - \mathbf{C}(\theta)] + \text{const.}, \quad (4.9)$$

where  $\hat{\mathbf{C}}$  and  $\Sigma$  are the data vector containing the tabulated values  $\{C_{\ell}\}$  and the covariance matrix derived from the 2018 Planck data [33].

### 4.1.2 Sampling

Sampling the parameter spaces investigated is performed by the GAMBIT scanner module `ScannerBit` [34]. Given a user-specified region in an  $n$ -dimensional parameter space, `ScannerBit` will choose  $n$  values from 0 to 1, which will constitute a point in an  $n$ -dimensional hypercube. This hypercube is then transformed to correspond to the physical  $n$ -dimensional space scanned. The  $n$  physical parameter values are then passed to a user-specified function, which is then used to perform the task at

hand [34].

In order to perform a scan the user must write a YAML file in which the parameter ranges and priors for the scan are indicated, what observables should be evaluated for each point scanned and what sampling method should be utilised [34]. In this thesis the most common choice of parameter ranges and priors have been to scan  $m_\chi$  and  $m_S$  in the regions (10 MeV, 100 GeV) or (1 GeV, 3 TeV) with a logarithmic prior and the other parameter values of interest being fixed. The crucial observable evaluated at each point has been the TT, TE and EE likelihoods for both low- $\ell$  and high- $\ell$ , which have been evaluated as described in section 4.1.1. The sampling method most commonly used in this thesis has been the differential evolution sampler Diver [34]. The practical implementation of these choices for the scans are described in section 4.2.5.

Diver makes use of a user-specified number of points in parameter space,  $\text{NP}$ , which makes up a population. The population is first initialised by a random selection of points in the parameter space, which makes up the first population generation. A population of points will be denoted  $\{\mathbf{X}_i^g\}$ , where  $g$  denotes the generation and  $i$  denotes a specific point in the population, i.e.,  $1 \leq i \leq \text{NP}$ . The next population generation will be selected through the following process. Each point in the population is assigned a random value  $F_i$ , such that  $F_l \leq F_i \leq F_u$ , where  $F_l = 0.1$  and  $F_u = 0.9$ . For each point in the population a random number,  $\tau_F$ , is generated between 0 and 1, and if  $\tau_F \leq 0.1$ , this point is assigned a new, random, value of  $F_i$  that fulfils the above condition. Next, for each point, three random points are selected from the population, denoted  $\mathbf{X}_{r1}^g$ ,  $\mathbf{X}_{r2}^g$  and  $\mathbf{X}_{r3}^g$  that fulfil  $\mathbf{X}_{rj}^g \neq \mathbf{X}_i^g$  and  $\mathbf{X}_{rj}^g \neq \mathbf{X}_{rk}^g$ . Each point is then assigned a *donor vector*,  $\mathbf{V}_i^g$  according to [34]

$$\mathbf{V}_i^g = \mathbf{X}_{r1}^g + F_i (\mathbf{X}_{r2}^g - \mathbf{X}_{r3}^g). \quad (4.10)$$

Next, each point is assigned a random value  $C_i$  that fulfils  $0 \leq C_i \leq 1$ . Similar to the process of selecting  $F_i$ , a random number between 0 and 1 is now selected,  $\tau_C$ , and if  $\tau_C \leq 0.1$ , a new  $C_i$  is sampled. For each dimension in the parameter space,  $k$ , a value  $r_k$  is generated such that  $0 \leq r_k \leq 1$ . This set of values is used to determine a trial vector,  $\mathbf{U}_i^g$ . For each dimension in the parameter space, if  $r_k \leq C_i$ , the  $k$ th value of the trial vector takes the value of the  $k$ th value of the donor vector, i.e.,  $\mathbf{U}_{i,k}^g = \mathbf{V}_{i,k}^g$ . If, on the other hand,  $r_k > C_i$ , the  $k$ th value of the trial vector takes the value of the  $k$ th value of the original point vector, i.e.,  $\mathbf{U}_{i,k}^g = \mathbf{X}_{i,k}^g$ . When this is done for all dimensions, in order to ensure the trial vector is always different from the original point vector, one dimension is chosen at random,  $l$ , and the  $l$ th component of the trial vector is assigned to the value of the donor vector, despite what the original assignation was, i.e.,  $\mathbf{U}_{i,l}^g = \mathbf{V}_{i,l}^g$ . When the above procedure has been performed for each point in the population, a trial population has been selected,  $\{\mathbf{U}_i^g\}$ . At each point in both the original population and the trial population, a function evaluating the *fitness parameter* is used, in the case of this thesis, this is the likelihood evaluation as described in section 4.1.1. For each point the fitness is compared to that of the new trial point and the one with the best fitness, i.e. highest value, is selected for the next population generation,  $\{\mathbf{X}_i^{g+1}\}$

[34]. Note that the previously selected values of  $F_i$  and  $C_i$  are carried on to the next generation and are only re-sampled if the new  $\tau_F$  and  $\tau_C$  dictates it. This procedure is then repeated until the user-specified threshold has been reached. This threshold is achieved when  $\delta < \text{convthresh}$ , where `convthresh` is specified by the user and  $\delta$  is given by

$$\delta = \frac{1}{n} \sum_{i=j}^{j-n+1} \left[ 1 - \frac{\sum_{\text{population}} \log \mathcal{L}_{i-1}}{\sum_{\text{population}} \log \mathcal{L}_i} \right]. \quad (4.11)$$

Here  $i$  is the generation index,  $j$  is the current generation number and  $n$  is a *population smoothing length*, set to 10 by default [34].

## 4.2 Practical implementation

In this section, a detailed description of the practical implementation used to perform this thesis is given, which should allow readers to replicate the work done or use this approach as a template for further investigations. To provide structure to this section, a schematic, chronological description of the implementation is here briefly given.

The main program utilised in this thesis is GAMBIT [35] so the first step is to successfully install this with all the needed modules and backends. This step is described in section 4.2.1. The computations performed were enabled by resources provided by the Swedish National Infrastructure for Computing (SNIC) at Chalmers Centre for Computational Science and Engineering (C3SE), as such the specific setup of GAMBIT detailed in section 4.2.1 is based on the use of these resources. If other resources are available, the specific implementation will differ. When GAMBIT is successfully installed, additional files and functions needed to obtain the presented results is written, this includes files that makes use of existing functions to evaluate specific parameters and uses these parameters to evaluate likelihoods, etc. This step is carefully explained in section 4.2.2. The next step is to implement the Lagrangian for the model. This is done using FeynRules [22], which has been used to provide a CalcHEP file [36] to be used by the micrOMEGAs [23][24] backend of GAMBIT. This step is described in section 4.2.4. When the model Lagrangian is implemented in the micrOMEGAs backend of GAMBIT and all functions needed for the calculations are written, GAMBIT can be executed with a YAML file, describing specific parameters and conditions to be implemented. How these files are written is explained in section 4.2.5.

### 4.2.1 Setting up GAMBIT

In order to build GAMBIT the following need to be installed;

- `g++/gfortran 5.1` or `icpc/ifort 15.0.2`

- **CMake 2.8.12**
- **Python 2.7** or **Python 3**
- Python modules: **yaml**, **os**, **re**, **datetime**, **sys**, **getopt**, **shutil** and **iter-tools**
- **git**
- **Boost 1.41**
- GNU Scientific Library (**GSL**) **2.1**
- **Eigen 3.1.0**
- **LAPACK**
- **pkg-config**
- 16 GB of RAM

Later versions of above mentioned packages may be supported by GAMBIT, but may require later versions of other packages. In order to compute the impact of annihilating DM on the CMB power spectrum, CosmoBit [2] is utilised. In order to run CosmoBit some Python packages must also be installed;

- **cython** (needed by **classy**)
- **scipy** (needed by **MontePython** and **DarkAges**)
- **numpy 1.12** or greater (needed by **DarkAges** and **classy**)
- **dill** and **future** (needed by **DarkAges**)
- **pandas** and **numexpr** (needed by **MontePython**)

Working on the computing cluster Vera, provided by C3SE, the above mentioned tools and packages are already provided in the form of modules which must be loaded. The modules that were loaded in order to build GAMBIT and performing the subsequent steps are the following;

- **foss/2019b**
- **Python**
- **PyYAML**
- **Eigen**
- **CMake**
- **Boost**
- **GSL**
- **dill**
- **EasyBuild**
- **plc**
- **git**
- **pkg-config**
- **CastXML**
- **CFITSIO**
- **HDF5/1.10.5-serial**
- **h5py/2.10.0-serial-Python-3.7.4**

Additionally a few Python packages had to be installed;

- **future**
- **numexpr**
- **scipy**

Loading the above mentioned modules and installing the Python packages can be performed from the Vera login node by running

```
$ module load foss/2019b Python PyYAML Eigen CMake Boost GSL dill  
EasyBuild plc git pkg-config CastXML CFITSIO HDF5/1.10.5-serial  
h5py/2.10.0-serial-Python-3.7.4  
$ pip install --user scipy future numexpr
```

After loading these modules or otherwise assuring the required packages are installed on the system GAMBIT may be built. The easiest way to get started is by downloading the latest version of GAMBIT using git (at the time of writing, this is version 1.5). From the terminal this can be done by running

```
$ git clone https://github.com/GambitBSM/gambit_1.5 gambit
```

In the newly created `gambit` folder, a build directory should be made from which GAMBIT will be built. GAMBIT uses `cmake` to build, which allows for various flags to be passed to the command. Some useful flags may be `-DWITH_MPI=ON` `-DWITH_HEPMC=ON` `-DBUILD_FS_MODELS=all` to be added to the `cmake` command. It is also worth mentioning that when installing GAMBIT it might have issues finding certain backends, in particular Eigen. If this occurs one can add an additional flag in the `cmake` step with direction to the Eigen package. The above steps are performed by running

```
$ cd gambit  
$ mkdir build  
$ cd build  
$ cmake -DWITH_MPI=ON -DWITH_HEPMC=ON -DBUILD_FS_MODELS=all  
-DEIGEN3_INCLUDE_DIR=/apps/Vera/software/Core/Eigen/3.3.7/include ..
```

After this it is time to make the scanners to be used in the scans. This is performed by running

```
$ make -jn scanners
```

where `n` should be replaced by the number of cores that should be utilised in this step, e.g., `-j4` for utilising 4 cores. When the scanners are built, it is time to actually build GAMBIT. Using the same flags as above, this is done by running the following

```
$ cmake -DWITH_MPI=ON -DWITH_HEPMC=ON -DBUILD_FS_MODELS=all
```

## 4. Method

---

```
-DEIGEN3_INCLUDE_DIR=/apps/Vera/software/Core/Eigen/3.3.7/include ..  
$ make -jn gambit
```

Depending on the specific scans one wishes to perform with GAMBIT, corresponding backends need to be loaded. In this thesis, the needed backends are

- **alterbbn**, [37]
- **classy\_exo\_2.7.2**, [38]
- **darkages**
- **micromegas**, [24]
- **montepythonlike**, [39, 40]
- **multimodecode**, [41, 42, 43]
- **plc**, [33]
- **plc\_data**, [33]

These backends are loaded by running

```
$ make alterbbn classy_exo_2.7.2 darkages micromegas montepythonlike  
multimodecode plc plc_data
```

In order to load all backends the above line should be changed by

```
$ make backends
```

There are some examples provided in the git that can be tested after performing the above steps. These examples are located in the `yaml_files`. Running the example file `CosmoBit_quickStart.yaml` can be performed by running the below code from the `gambit` folder.

```
$ ./gambit -f yaml_files/CosmoBit_quickStart.yaml
```

To summarise the entire setup procedure, including testing the `CosmoBit_quickStart` file, after ensuring all prerequisites are met, the building and running of the test file (sufficient for the scans performed in this thesis) can be performed as written below

```
$ git clone https://github.com/GambitBSM/gambit_1.5 gambit  
$ cd gambit  
$ mkdir build  
$ cd build  
$ cmake -DWITH_MPI=ON -DBUILD_FS_MODELS=all -DWITH_HEPMC=ON  
-DEIGEN3_INCLUDE_DIR=/apps/Vera/software/Core/Eigen/3.3.7/include ...;  
$ make -j4 scanners  
$ cmake -DWITH_MPI=ON -DBUILD_FS_MODELS=all -DWITH_HEPMC=ON  
-DEIGEN3_INCLUDE_DIR=/apps/Vera/software/Core/Eigen/3.3.7/include ...;  
$ make -j4 gambit
```

```
$ make alterbbn classy_exo_2.7.2 darkages montepythonlike
multimodecode micromegas plc plc_data; cd ..
$ ./gambit -f yaml_files/CosmoBit_quickStart.yaml
```

The installation is further explained in [2],[35] or the `README` file provided in the above git.

It is further worth noting that in some cases this setup has issues finding the LAPACK module when installing the `plc` backend, heavily utilised in this thesis. If this occurs one can install it manually with the loaded modules by moving to the `/gambit/Backends/installed/plc/3.0` directory and running

```
$/waf configure --lapack_link=-lopenblas
$/waf install
```

after performing a failed `makeplc` attempt, which will have built the above folder.

## 4.2.2 Additional files in GAMBIT

The new model used in this thesis is named `AnnihilatingDM_Thesis`. It takes 6 parameters as input, namely the DM and mediator masses in GeV, `mass_DM` and `mass_med`, the three couplings  $\lambda_{\chi S}$ ,  $\lambda_{Sf}$  and  $\lambda_S$ , named `lambda_DM`, `lambda_med_ferm` and `lambda_med`, as well as a parameter named `version` which is used to select the model Lagrangian in question, `version=1` uses the Lagrangian eq. (3.13) with only electron-positron pairs as final states and `version=2` uses all fermion final states. The model can be used to evaluate likelihoods for comparison both to CMB data, when considering `version=1`, and to the expected value of the relic density,  $\Omega_\chi h^2 \approx 0.1188$  [29]. In order to compare to CMB data the model makes use of the existing parent model `AnnihilatingDM_general` from the CosmoBit module [2] to evaluate the effect annihilating DM has on the CMB power spectrum. This model takes the DM mass in GeV and annihilation cross section in  $\text{cm}^3\text{s}^{-1}$  as inputs. In order to provide the cross section given the input parameters, a function provided by the micrOMEGAs [24] backend of GAMBIT, `vSigma` [24], is used. Similarly, in order to evaluate the relic density another function from the micrOMEGAs backend, `darkOmega` [23], is used. For the micrOMEGAs backend to perform these calculations a description of the BSM Lagrangian used must be provided in a CalcHEP file [36]. How this has been done is described in section 4.2.4.

The practical implementation in the code is here described. The model `AnnihilatingDM_Thesis` is defined in the file `gambit/Models/src/models/CosmoEnergyInjection.cpp` as written in appendix A.1.1. Here a yet-to be written function called `CalculateSigmaV` is called, in which the thermally averaged annihilation cross section should be calculated. This function is defined in the same file and written as in appendix A.1.2. This function calls yet-to be written files in the micrOMEGAs backend, which will perform the actual calculations. In order to enable parallel execution, i.e., several cores performing these calculations

simultaneously for different parameter values, the evaluated value of the cross section is saved to an external file in the temporary directory, named with regards to the value of the DM mass of the particular scan. The additional files needed to perform the calculations are described in section 4.2.3. Now that the shell of the model has been written, it is declared in the file `gambit/Models/include/gambit/Models/models/CosmoEnergyInjection.hpp` as written in appendix A.1.3. The next thing to do is to write the function

`energy_injection_spectrum_AnnihilatingDM_Thesis` which contains the injected spectra of  $e^+e^-$  pairs. This is done in the CosmoBit backend of GAMBIT and is defined in the file `gambit/CosmoBit/src/CMB.cpp` as written in appendix A.1.4. Note that it is assumed that the only final state is  $e^+e^-$ , and that this function is identical to the provided function `energy_injection_spectrum_AnnihilatingDM_mixture`, apart from the fact that the branching ratio of electrons is set to 1 and the branching ratio to photons is set to 0. The function is declared in the file `gambit/CosmoBit/include/gambit/CosmoBit/CosmoBit_rollcall.hpp` under the capability `energy_injection_spectrum` as written in appendix A.1.5.

The above implementation is sufficient to evaluate regions in parameter space that are excluded by CMB data. If one wants to instead compare to the expected value for the evaluated relic density additional functions must be written. Functions for evaluating the likelihood when comparing to the relic density are already implemented in `gambit/DarkBit/src/SimpleLikelihoods.cpp` and is named `nL_oh2_Simple`, alternatively `nL_oh2_upperlimit`. What remains is then to write a new function evaluating the relic density for the new model. To do this, a new function is added in `gambit/DarkBit/src/RelicDensity.cpp` as written in appendix A.1.6 and a capability to the existing function is added in `gambit/DarkBit/include/gambit/DarkBit/DarkBit_rollcall.hpp` under the capability `RD_oh2` as written in appendix A.1.7.

By default the complete program will only save certain parameters, such as the input parameters and evaluated likelihoods. In order to save additional parameters, such as the annihilation cross section and the relic density, additional functions must be written. These functions have been added to the file `gambit/CosmoBit/src/Planck.cpp` as written in appendix A.1.8. Note that these functions make use of the previously used functions `CalculateSigmaV` and `CalculateOmega` as written in appendix A.1.2 and appendix A.1.6. These functions can be added locally to this file if one does not wish to connect this file to the ones in which they were already defined. In order to access these functions externally, they need to be added to `gambit/CosmoBit/include/gambit/CosmoBit/CosmoBit_rollcall.hpp` as done in appendix A.1.9.

When the above implementations to GAMBIT have been made, it needs to be rebuilt to incorporate these changes. This is done by executing the following steps from the gambit directory;

```
$ rm -rf build
```



```

$ mkdir build
$ cd build
$ cmake -DWITH_MPI=ON -DWITH_HEPMC=ON -DBUILD_FS_MODELS=all ..
$ make -j4 scanners
$ cmake -DWITH_MPI=ON -DWITH_HEPMC=ON -DBUILD_FS_MODELS=all ..
$ make -j4 gambit
$ make alterbbn classy_exo_2.7.2 darkages montepythonlike
multimodecode micromegas plc plc_data; cd ..

```

### 4.2.3 Additional files in the micrOMEGAs backend

For the actual computation of the thermally averaged annihilation cross section and the relic density the micrOMEGAs backend is used [24]. In this backend, i.e., `gambit/Backends/installed/micromegas/3.6.9.2/` one can create new projects by running the command `./newProject <ProjectName>`. For this thesis two separate projects have been made, named `Spin0` and `Validation0`, which will contain the model Lagrangian eq. (3.13) for the cases where the final states are only electron-positron pairs and all fermion-antifermion pairs, respectively. Creating these new projects makes template folders for the user to fill with the model in question. This was in this thesis done using an external program FeynRules [22] and is explained in section 4.2.4. This section describes the files written in the micrOMEGAs backend that have already been called by functions written in the above section. The files are identical for the two projects created and when referring to specific files it will be referred to the `Spin0` project for simplicity.

In the new project folder a main script is created `.../Spin0/main.c` which evaluates several parameters for the model in question. In this thesis only two parameters are of interest, the annihilation cross section and the relic density and these parameters must be saved such that the functions in GAMBIT can access them. To this end two new files are created, `.../Spin0/omega.c` and `.../Spin0/sigmav.c`.

The file `omega.c` makes use of the micrOMEGAs function `darkOmega` [23], which evaluates the relic density for the given model and also evaluates the freeze-out temperature. It then saves the evaluated relic density to an external file named `omegasave_<mDM>.txt`, where the dark matter mass is used to identify the parameter file when running multiple cores at once. The file `omega.c` is called by various GAMBIT functions and after collecting the value from the parameter file, this parameter file is deleted. The file is written as in appendix A.2.1.

The file `sigmav.c` makes use of the micrOMEGAs function `vSigma` [24], which evaluates the thermally averaged annihilation cross section in pb. It needs the temperature in GeV as input and to this end the freeze-out temperature evaluated by `darkOmega` is used. Similar to for `omega.c`, the evaluated cross section (in  $\text{cm}^3\text{s}^{-1}$ ) is saved to an external file, which is then deleted once it has been collected by the GAMBIT functions. The file is written as in appendix A.2.2.

The executables that are used by the main GAMBIT files are then created by running

```
$ gmake main=omega.c
$ gmake main=sigmav.c
```

in the `Spin0` directory.

### 4.2.4 Implementing the Lagrangian

The Lagrangian is expressed in a FeynRules file [22]. The first step is to download FeynRules, which can be done from <https://feynrules.irmp.ucl.ac.be/>. This should provide a folder named `feynrules-current`, which can be placed in the same directory as the `gambit` folder. For this thesis the evaluated model Lagrangian is expressed in the existing file `feynrules-current/Models/SM/SM.fr` as described in appendix A.3.1. The model is then expanded to CalcHEP files [36] and sent to the micrOMEGAs backend using a Mathematica notebook as written in appendix A.3.2.

### 4.2.5 Executing the program

In order to perform a scan using GAMBIT a YAML file should be written specifying the details of the scan. In the downloaded directory `gambit/yaml_files/` there are several example files, in particular `CosmoBit_quickStart.yaml` and `CosmoBit_tutorial.yaml` can be very helpful and have been used as guidelines for setting up the YAML files used for this thesis. The YAML files are in general composed of the following sections; **Parameters**, **Printer**, **Scanner**, **ObsLikes**, **Rules**, **Logger** and **KeyValues**. In the **Parameter** section all parameters needed for the particular scan are defined, this includes fixed values needed for particular models as well as ranges and priors for parameters to be scanned over. The **Printer** section includes information about how the data should be printed, i.e., to what format. In this thesis the HDF5 printer has been used. The **Scanner** section includes information necessary for the sampling algorithm. The scanner Diver [34] has been used in this thesis, as explained in section 4.1.2. In the section **ObsLikes** all the observables that should be evaluated in the scan should be declared. The observables can either be declared as **LogLike**, meaning they are used to drive the scan, i.e., they are used as fitness parameters in the scan, or **Observable**, meaning they should just be saved to the output. In the **Rules** section descriptions are added to determine how the above observables should be evaluated, if needed, as well as settings related to specific backends. The **Logger** and **KeyValues** sections should include information regarding if, how and where certain outputs should be stored. Two examples are provided in appendix A.4.1 and appendix A.4.2, illustrating how such a YAML file can be written in the case of evaluating allowed regions in the  $(m_\chi, m_S)$ -space when comparing to CMB data and relic density data, respectively.

## 4.3 Obstacles

In this section some of the obstacles encountered while performing this thesis are highlighted. The focus lies on issues regarding the practical implementation, section 4.3.1, and the choice of parameter space to scan over, section 4.3.2.

### 4.3.1 Practical implementation

Using a cluster to perform the jobs, many problems have been encountered when trying to find the correct modules to load in order to build GAMBIT successfully. Even when a given set of modules have been loaded and GAMBIT has seemed to be built correctly, there have still been times when jobs have crashed because of the loaded modules. In more than one occasion certain modules seemed to be adequate and simple jobs presented no issues, but when trying to perform longer jobs that were of actual interest for this thesis the job could run flawlessly until the very end, when the data should be saved to a new file, where the program crashed. Since such programs need to run for a substantial amount of time to be able to produce significant results, such issues have definitely hindered the work. Finally a set of modules that worked were found, which were presented in section 4.2.1.

### 4.3.2 Parameter space

In order to perform jobs that will yield good result, the ranges chosen on the parameter space is important. In this subsection a few potential issues related to the choice of scanned parameter space are illustrated.

#### 4.3.2.1 Sampling

How the sampling is performed is explained in section 4.1.2. If the selected parameter space is too large, several issues related to the sampling of the parameter space can be encountered. One example is that the sampler might get stuck in a local minimum and not reach global minimum. An example of this is when comparing to the correct value of the relic density, which should only occur in a narrow region in parameter space. In such a narrow range it is very likely only a fraction of the possible values will be sampled in the parameter space. Another issue is when comparing to data which yields large regions with very similar value of the evaluated likelihood, e.g., when comparing to CMB data. In this case the most interesting aspect is the transition from high to low likelihood, but this region is less likely to be sampled, meaning the transition might be poorly sampled and not yield detailed results.

#### 4.3.2.2 Limits

As already mentioned above, selecting a parameter space that is too large may lead to issues for the sampler that will hinder the scan from obtaining detailed results. Another issue with selecting too large parameter spaces is that it may be possible to sample points in the parameter space that are very un-physical and lead to problems evaluating certain parameters. In order for the program not to crash in the event

#### 4. Method

---

of such points in the parameter spaces being sampled, the functions written in this thesis will return very poor values of the selected parameter instead of NaN.

# 5

## Results

The impact of annihilating DM has been investigated for two separate observables; the DM relic density and the CMB power spectrum. The results are first presented separately; results obtained from comparison to the observed DM relic density are presented in section 5.1, after which the results obtained from comparison to the observed CMB power spectrum are presented in section 5.2. The combined constraints are presented in section 5.3 and finally a description of how the confidence limits for the CMB data was set is given in section 5.4.

### 5.1 Relic density

The results obtained by comparing to the observed relic density are here presented. In section 5.1.1 the evaluated relic density for the model is compared to previous result to validate the model and its implementation. In section 5.1.2 the relic density is used to set constraints on the model when only considering  $e^+e^-$  final states, which can then be compared to results obtained by comparing to the theoretical impact on the CMB power spectrum.

All scans performed to obtain the results presented in this section utilised the Diver sampler, as described in section 4.1.2, with a population size of 20.000 and `convthresh`= 0.001. All scans were performed on 64 cores and obtained the final data set of 200.000+ data points after approximately 20 – 30 minutes.

#### 5.1.1 Validation

The investigated model Lagrangian, eq. (3.13), was considered as a potential SM extension in [15]. For fixed sets of values of the coupling constants,  $(\lambda_\chi, \lambda_{Sf}, \lambda_S) = (1, 0.25, 1), (1, 1, 1), (0.25, 1, 1)$ , the parameter space  $(m_\chi, m_S)$  was investigated to identify regions where the obtained DM relic density is in agreement with the observed value  $\Omega_\chi h^2 \approx 0.1188$ . The results from this investigation is presented in fig. 10 in [15]. To validate the implementation of the model Lagrangian in this thesis, the same investigation was performed and should be compared to the previous work. The results from this investigation are presented in fig. 5.1, where points in the parameter space that yielded  $\Omega_\chi h^2 \in [0.9 \cdot 0.1188, 1.1 \cdot 0.1188]$  are presented in red. The figures include the results from two separate scans, one in the region  $m_\chi, m_S \in [1, 2000]$  GeV with flat priors and one in the region  $m_\chi, m_S \in [1, 500]$  GeV with logarithmic priors, the reason for this was to obtain more valid sampled points

at lower masses, where the region of valid points is very narrow. Comparing the results obtained here to the results presented in fig. 10 in [15], good agreement can be seen, effectively validating the implementation of the model Lagrangian and the evaluation of the relic density for given parameter values.

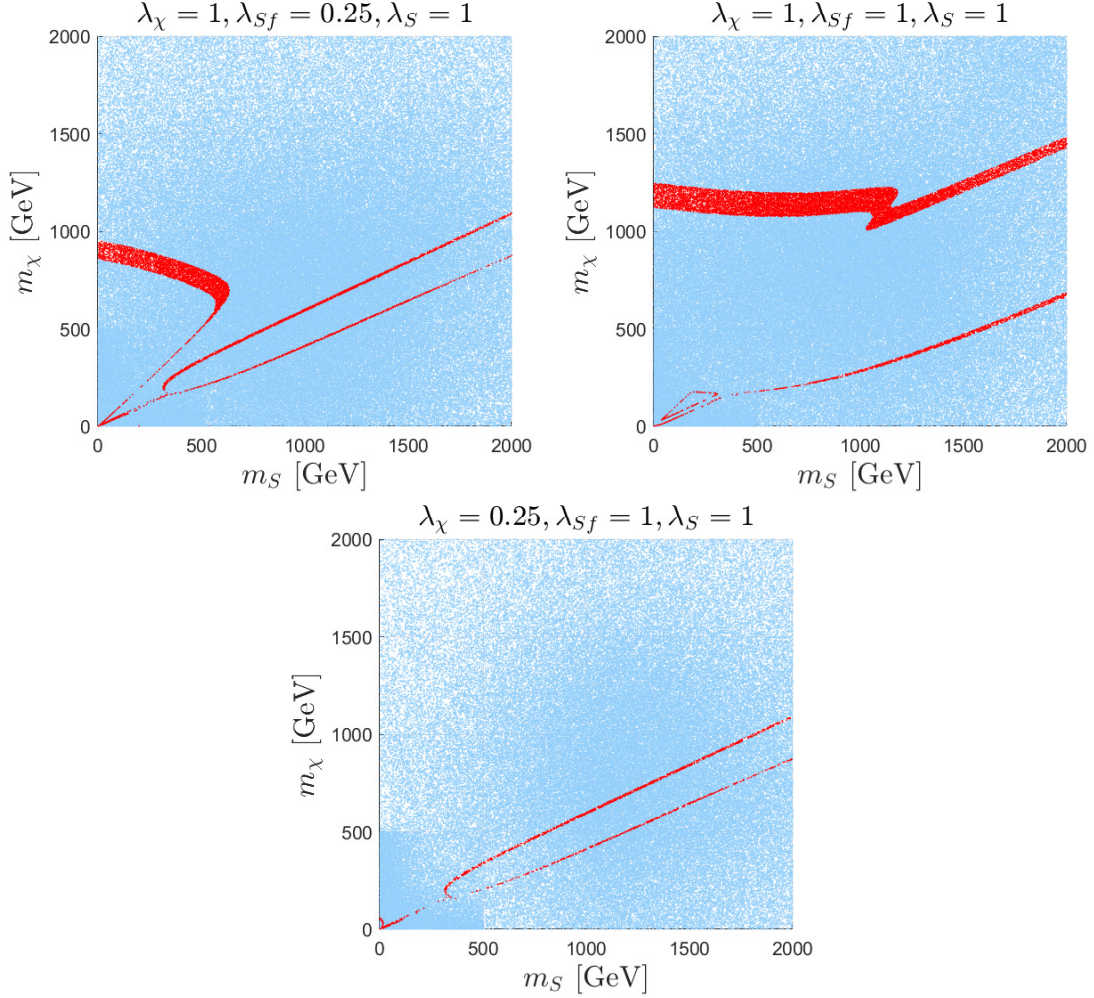


**Figure 5.1:** Constraints on the parameter space  $(m_\chi, m_S)$  set by obtaining the correct value of the relic density ( $\pm 10\%$ ) illustrated in red. All sampled points are illustrated for reference in blue. The three figures respectively indicate the regions of correct relic density when considering  $(\lambda_\chi, \lambda_{Sf}, \lambda_S) = (1, 0.25, 1), (1, 1, 1), (0.25, 1, 1)$ . The results were obtained when implementing all final states in eq. (3.13) and should be compared to the results presented in fig. 10 in [15].

### 5.1.2 Parameter constraints

In addition to evaluate the relic density when the model is given by eq. (3.13) with all fermionic final states accessible, as presented in section 5.1, it was also investigated how the allowed regions in the parameter space  $(m_\chi, m_S)$  would change when only allowing the  $e^+e^-$  final state. The results are presented in fig. 5.2.

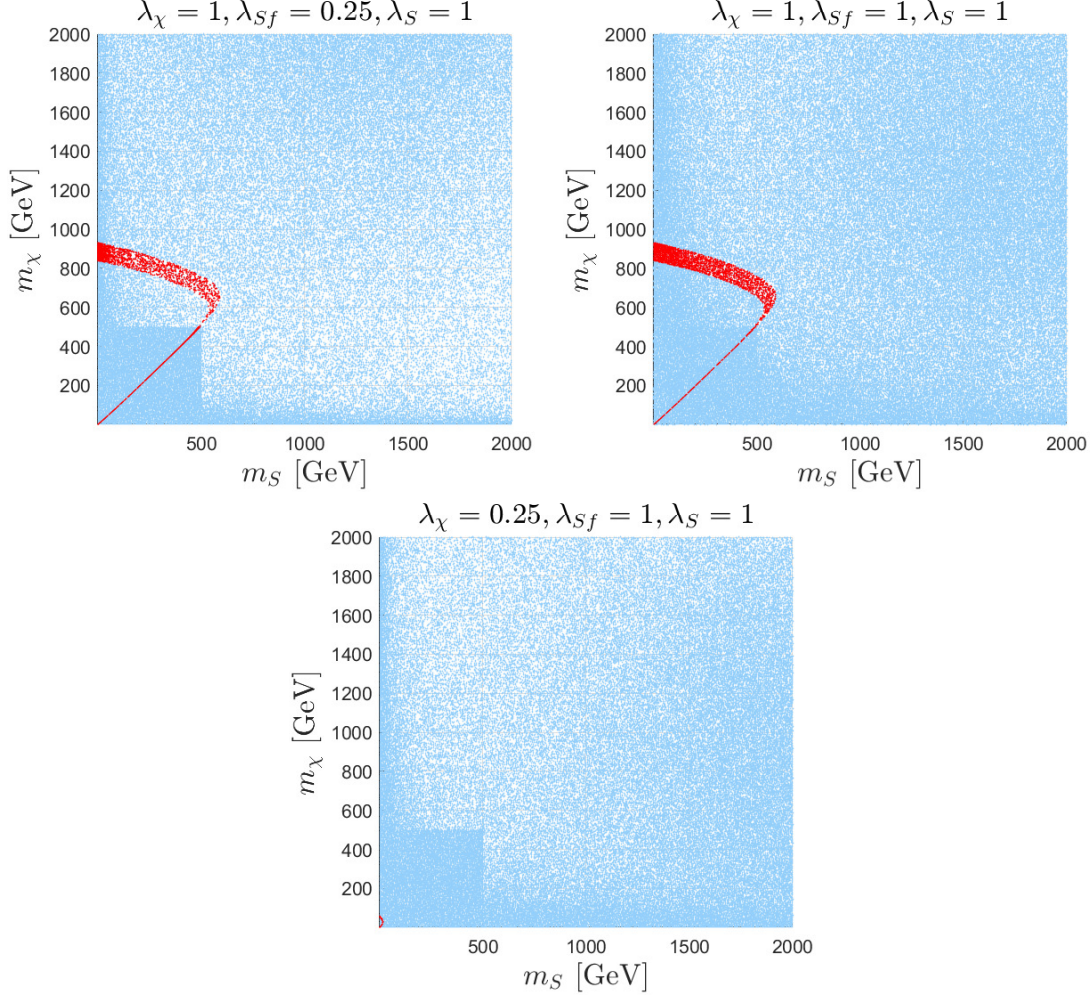


**Figure 5.2:** Same as fig. 5.1, but only implementing  $e^+e^-$  final state in eq. (3.13).

It is clear that constraining the model to only include the  $e^+e^-$  final state affects the region in which the correct DM relic density is obtained. It is also clear it would be of interest to investigate regions of lower masses. Equivalent scans are therefore performed in regions fulfilling  $m_\chi, m_S \in (10^{-2}, 3 \cdot 10^3)$  GeV. The combined results from the different scans are presented in fig. 5.3. In fig. 5.3 the regions in parameter space where the evaluated relic density is larger (excluded) and smaller (not necessarily excluded) than the observed value are distinguished from one another. Note that the presented results have been obtained by identifying a connected region corresponding to the limiting case, which has been used to divide the parameter space. This procedure has been implemented for the following results in this chapter as well. Results illustrating all sampled points have been provided in appendix B for



comparison. In addition, the relic density has been evaluated for different values of  $m_\chi$  when varying  $m_S$ . The results from these scans are presented in fig. 5.4, with the limiting value,  $\Omega_\chi h^2 = 0.1188$ , indicated. Note that the excluded regions coincide with the regions where the evaluated relic density is larger than the observed value.

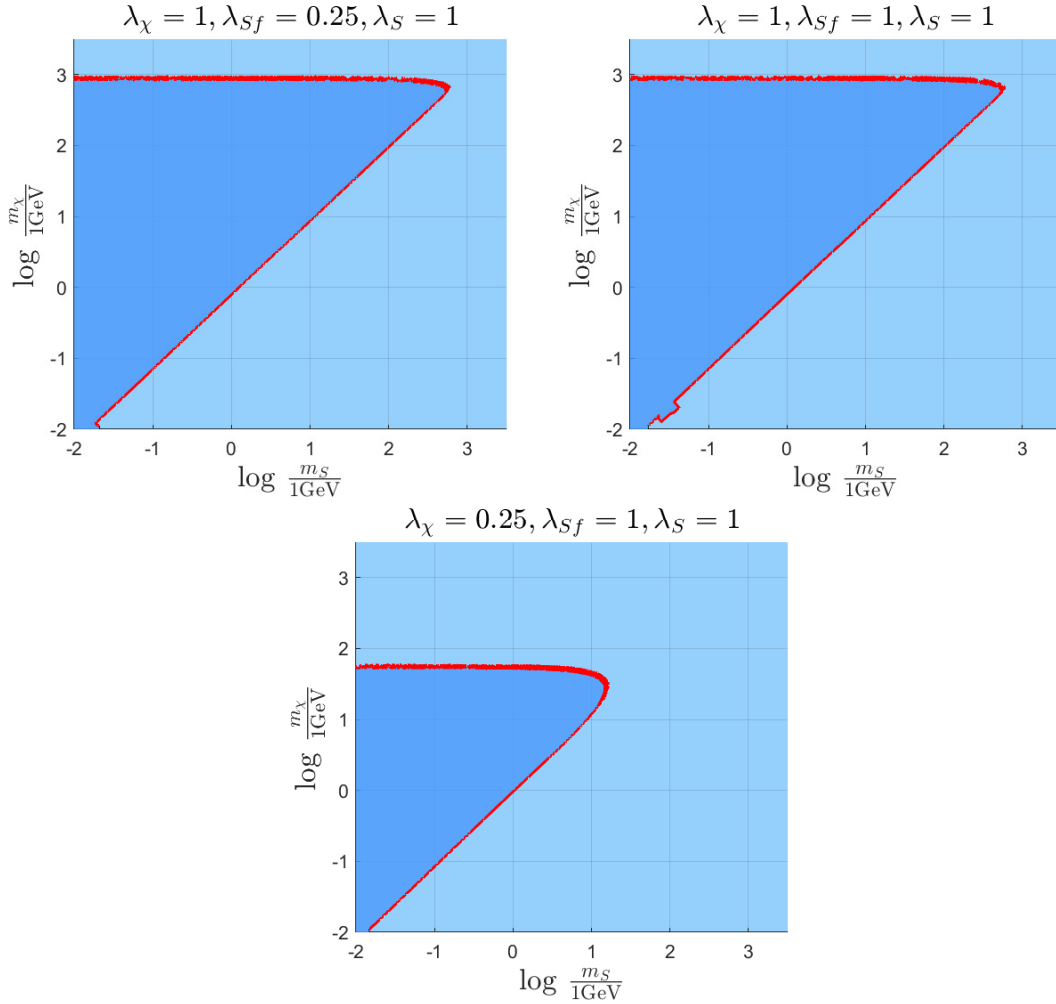


**Figure 5.3:** Same as fig. 5.2, but for mass ranges  $m_\chi, m_S \in (10^{-2}, 3 \cdot 10^3)$  GeV. In addition the region in parameter space where the evaluated relic density is smaller than the observed is highlighted in a darker shade of blue, while the region where the evaluated relic density is larger than the observed value is illustrated in lighter shade of blue. The data used to obtain these results is illustrated further in fig. B.1 and fig. B.2.



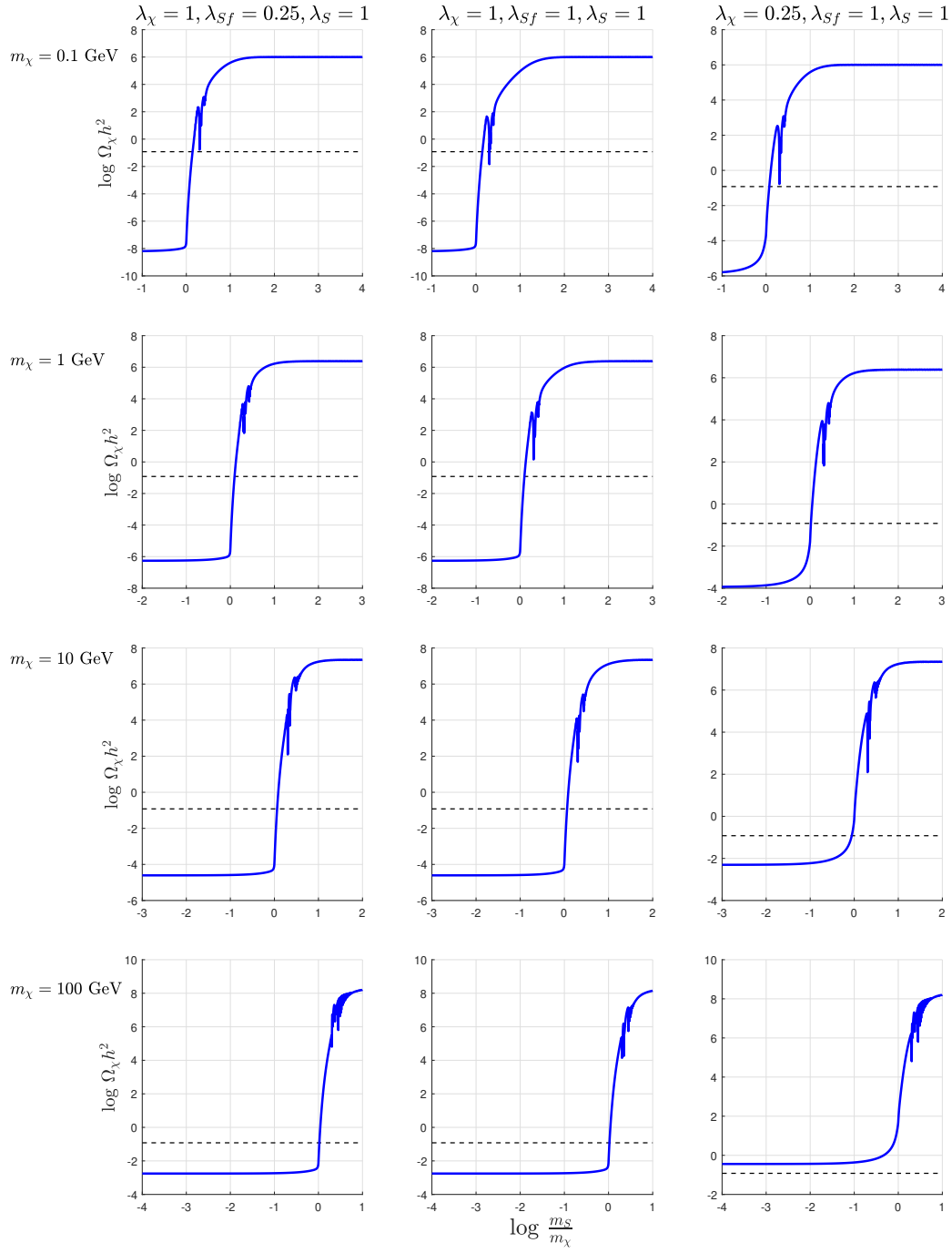


**Figure 5.4:** The evaluated relic density as function of  $\frac{m_S}{m_\chi}$  for different values of  $m_\chi$ . The observed limit  $\Omega_\chi h^2 = 0.1188$  is included as black dashed lines.

## 5.2 Cosmic microwave background

The results obtained by comparing to the observed CMB power spectrum are here presented. In section 5.2.1 the allowed region in the  $(m_\chi, \langle\sigma v\rangle)$  parameter space is investigated and compared to previous results to validate the implementation of energy injection and calculation of the CMB power spectrum. In section 5.2.2 the observed CMB power spectrum is used to set constraints on the model.

All scans performed to obtain the results presented in this section utilised the Diver sampler, as described in section 4.1.2, with a population size of 10.000 and `convthresh`= 0.001. All scans were performed on 128 cores and obtained the final data set of 100.000+ data points after approximately 16 hours.

### 5.2.1 Validation

Using the CMB likelihood as provided by `plc`, nuisance parameters are needed. If restricting the use to the 'lite' versions, only one nuisance parameter is needed,  $A_{\text{planck}}$ , as explained in section 4.1.1. When included, this parameter is scanned with a flat prior in the range  $[0.9, 1.1]$  by default. However, this affects the theoretical power spectra greatly, and drastically reduces the predictive power of the parameter scan. To illustrate this point, the results from three separate scans for the parent model `AnnihilatingDM_general` are shown in fig. 5.5 with different ranges for  $A_{\text{planck}}$ . Note that these scans took approximately 16 hours to complete. To ensure results were obtained in reasonable time for the completion of this thesis it was opted to set the nuisance parameter to 1 for the appropriate CMB scans.

The authors of the backend CosmoBit have used the CMB power spectrum to identify excluded regions in the  $(m_\chi, \langle\sigma v\rangle)$  parameter space [2]. In order to validate the implementation of the energy injection and the resulting CMB power spectrum as performed in this thesis, similar scans were performed and the results are presented in fig. 5.6. By comparison with fig. 9 in [2], the implementation is considered to be correct. Note that results from two separate scans are presented in the same figure, as the scans encountered issues when trying to sample the entire parameter space at once. The procedure of obtaining the 95% confidence limit of the excluded region is described in section 5.4.

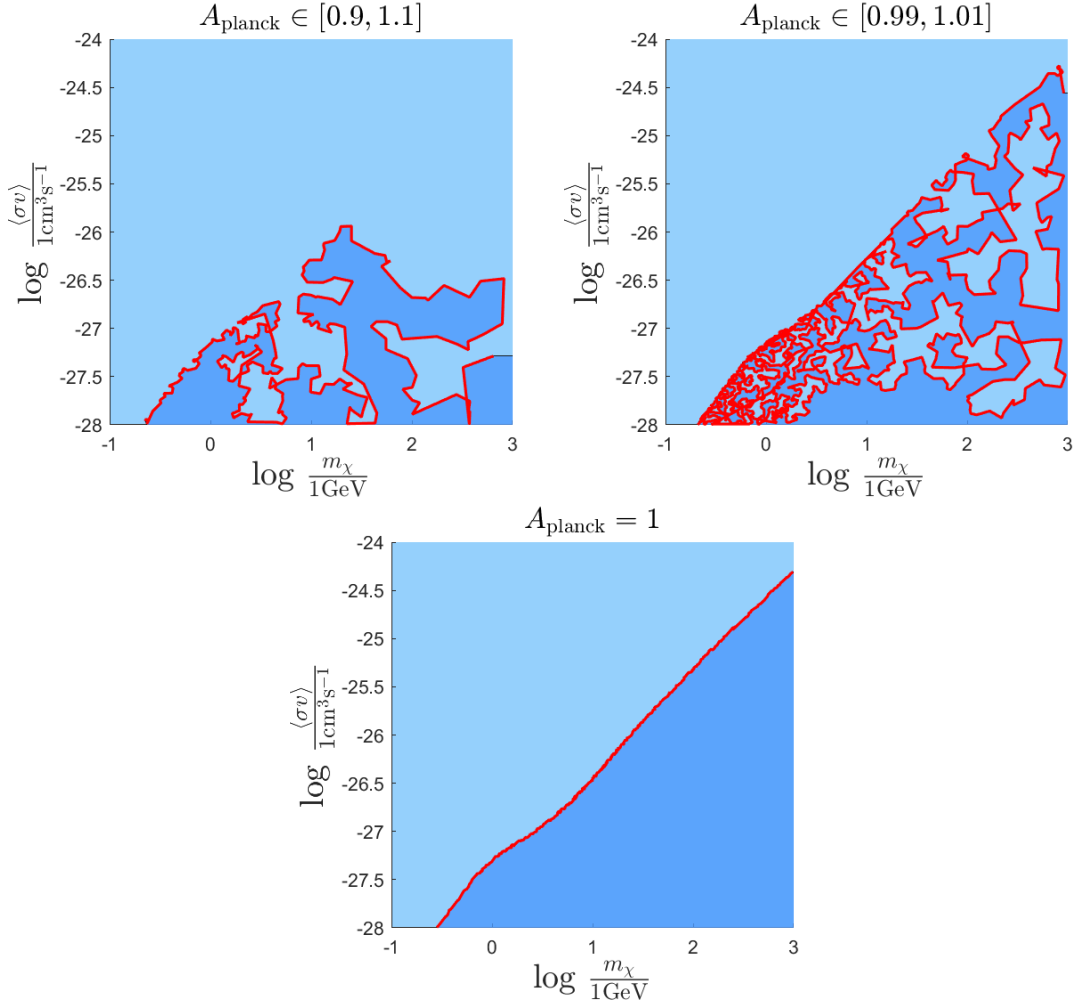


**Figure 5.5:** Likelihood plots in the  $(m_\chi, \langle\sigma v\rangle)$  parameter space for different ranges of the nuisance parameter  $A_{\text{planck}}$ . In the upper left plot the default range was used, i.e.,  $A_{\text{planck}} \in [0.9, 1, 1]$ . In the upper right plot a more restricted range was used,  $A_{\text{planck}} \in [0.99, 1, 01]$ . In the bottom plot the value was fixed to  $A_{\text{planck}} = 1$ . The figures illustrate attempts at identifying excluded regions (light blue) with 95% confidence as explained in section 5.4. The fragmented structure of the first two scans implies the scans were unsuccessful in identifying regions of agreeable values of  $A_{\text{planck}}$  before terminating. The data used to obtain these results is illustrated further in fig. B.3.

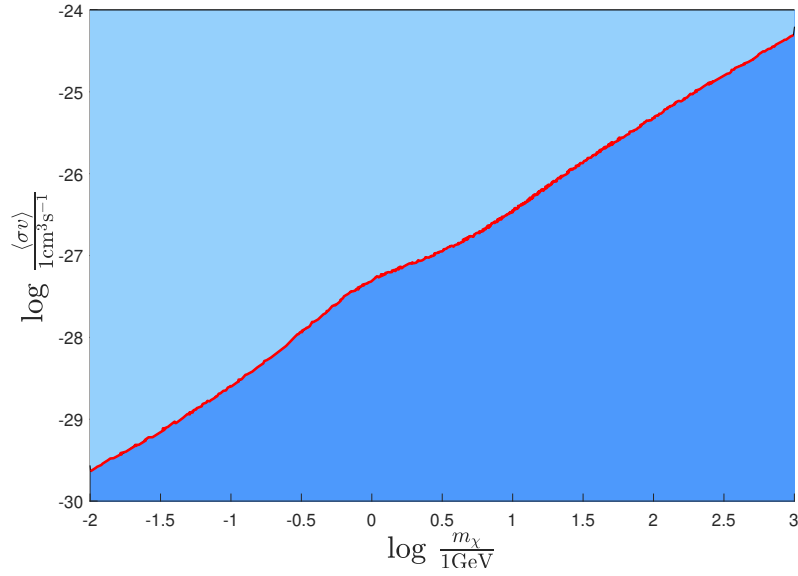


**Figure 5.6:** Constraints on the parameter space  $(m_\chi, \langle\sigma v\rangle)$  when studying the CMB power spectrum. The points illustrated in a lighter shade of blue make up the excluded region with 95% confidence, evaluated as described in section 5.4. These results should be compared to fig. 9 in [2]. The data used to obtain these results is illustrated further in fig. B.4.

### 5.2.2 Parameter constraints

Using the DM model as validated in section 5.1.1 and the effects of the energy injection as validated in section 5.2.1, the constraints on the model set by the CMB power spectrum was evaluated. The results are presented in fig. 5.7 and show the excluded region in the  $(m_\chi, m_S)$  parameter space with a 95% confidence limit, obtained as described in section 5.4. Investigating the properties of the region at lower masses the annihilation cross section for different values of  $m_\chi$  was evaluated when varying  $m_S$ . The results from these scans are presented in fig. 5.8, with the limiting value of the cross section, as obtained from fig. 5.6, indicated. Note that the excluded regions coincide with the regions where the evaluated cross section is too large for the impact on the power spectrum to be negligible, i.e., for cross section larger than the indicated values.

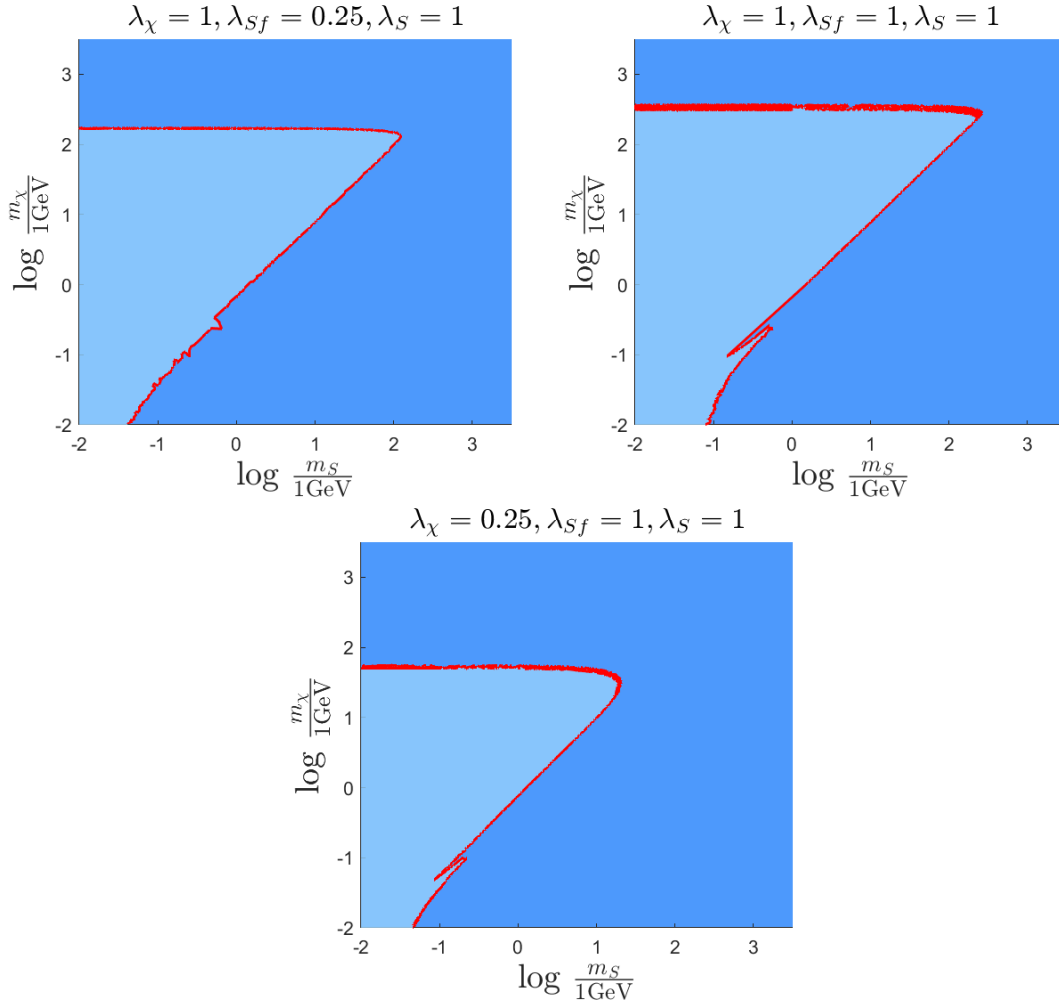


**Figure 5.7:** Likelihood plots in the  $(m_\chi, m_S)$  parameter space in the ranges  $m_\chi, m_S \in [10^{-2}, 3 \cdot 10^3]$  GeV for different sets of coupling strengths when comparing to CMB data. The excluded region with 95% confidence is indicated in light blue. The sets of coupling strengths investigated were  $(\lambda_\chi, \lambda_{Sf}, \lambda_S) = (1, 0.25, 1), (1, 1, 1)$  and  $(0.25, 1, 1)$  for the upper left, upper right and bottom plot respectively. The data used to obtain these results is illustrated further in fig. B.5 and fig. B.6.

## 5. Results

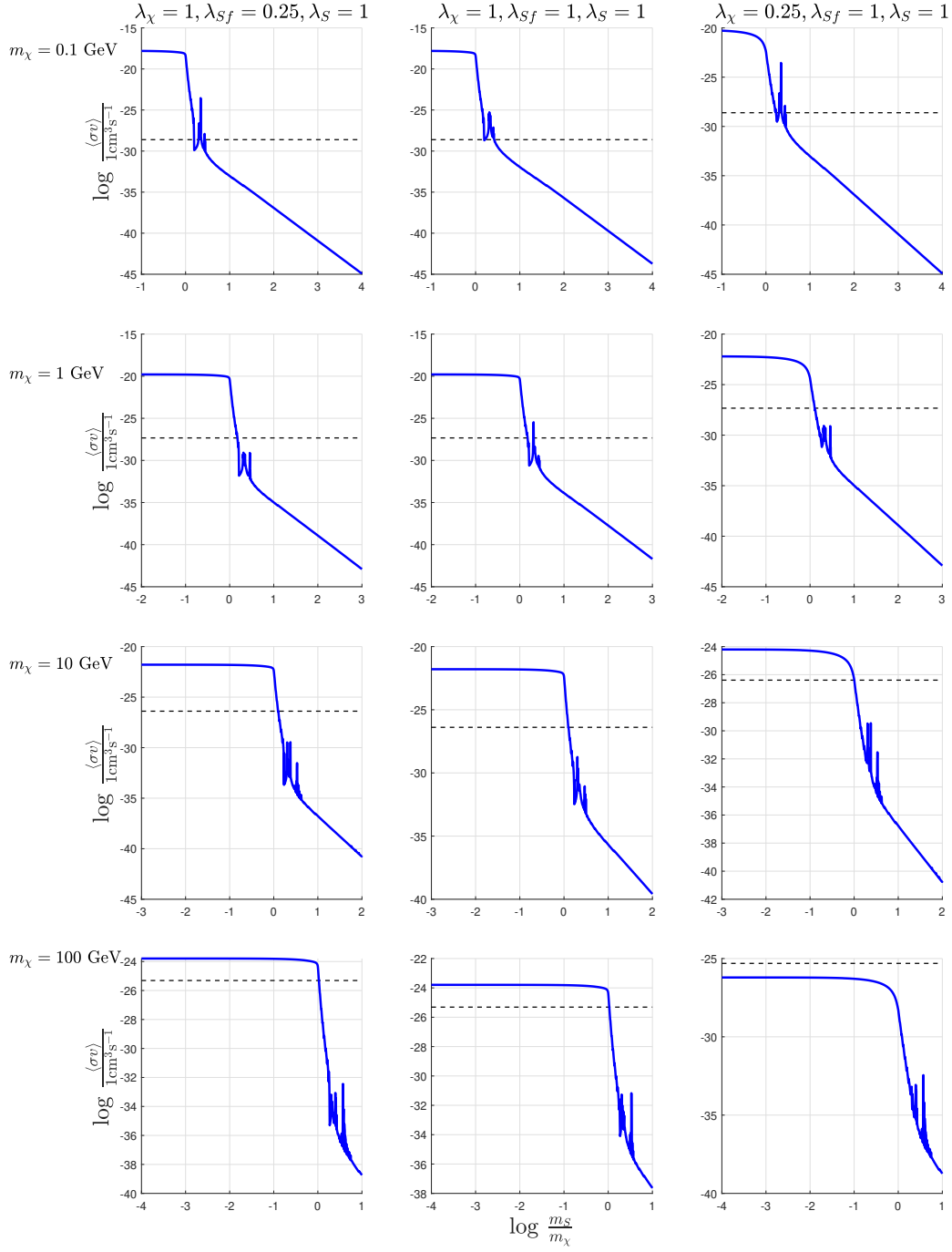


**Figure 5.8:** The evaluated annihilation cross section as function of  $\frac{m_S}{m_\chi}$  for different values of  $m_\chi$ . The evaluated limits of the cross section at the respective values of  $m_\chi$ , as indicated by fig. 5.6, are included as black dashed lines.

### 5.3 Combined constraints

In this section the combined constrained obtained in the previous sections are investigated. The results containing the combined excluded region from both relic density and CMB data in the parameter space  $m_\chi, m_S \in [10^{-2}, 3 \cdot 10^3]$  GeV are presented in fig. 5.9.

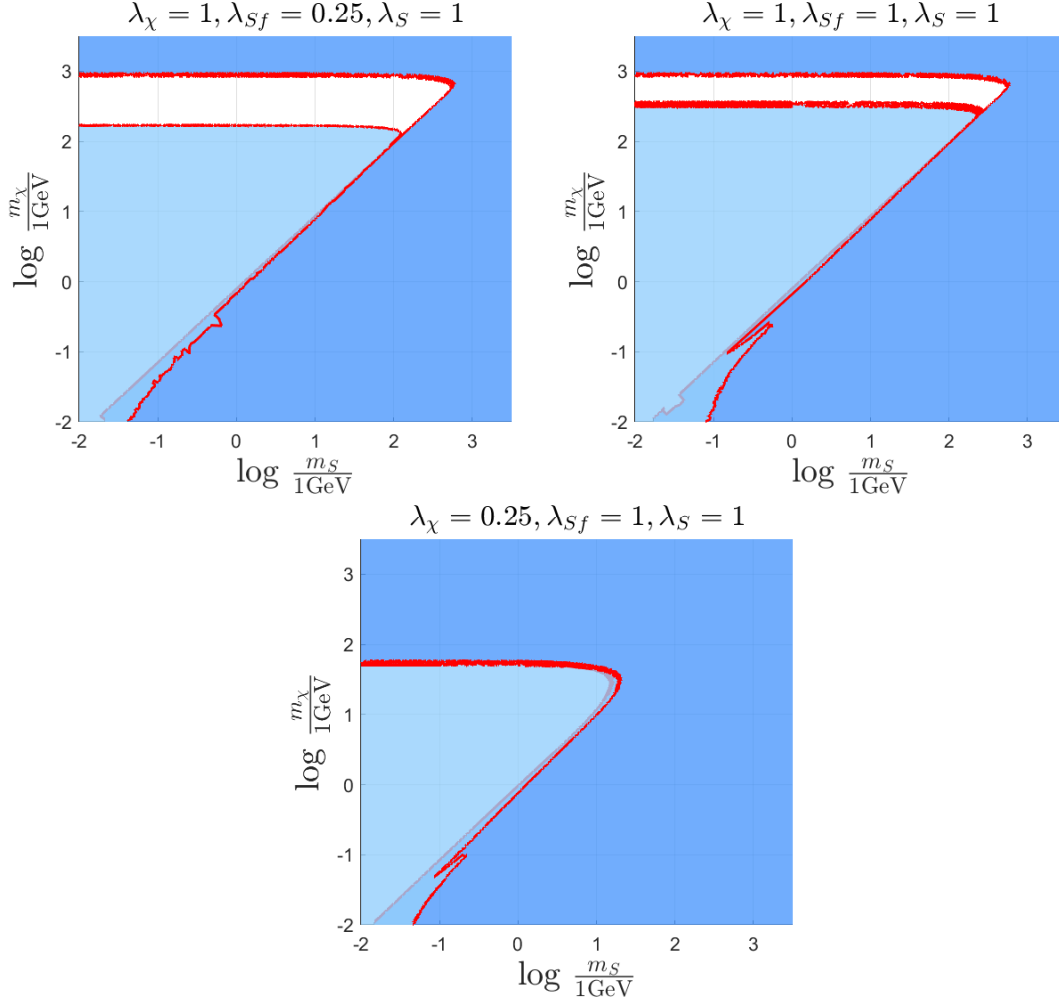


**Figure 5.9:** The combined excluded regions from both relic density and CMB data. The regions that are excluded for yielding DM relic density that is too large is illustrated in dark blue, while the regions that are excluded from CMB data is illustrated in light blue. The white regions are not excluded. The data used to obtain these results is illustrated further in fig. B.7.

## 5.4 Confidence interval

In order to quantitatively express bounds on the parameter space in the absence of a strict limit, as done in section 5.2, it is in this section explained how the confidence interval of the results presented in this chapter were obtained.

After successfully scanning a certain parameter space the obtained data will contain a set of points with a distribution of evaluated likelihoods,  $\log \mathcal{L}(\theta)$ , where  $\theta$  is the set of parameter values used as inputs. Focusing on the negative log likelihood,  $\chi^2(\theta) = -\log \mathcal{L}(\theta)$ , the "best fit" in this data set can be identified as

$$\chi_{\min}^2 = \min \left( \chi^2(\theta) \right). \quad (5.1)$$

A new distribution can then be constructed as [44]

$$\Delta\chi^2(\theta) = \chi^2(\theta) - \chi_{\min}^2.$$

For a typical scan this distribution will resemble that presented in fig. 5.10. This distribution follows a  $\chi_1^2$ -like distribution and the 95% confidence regions were evaluated as

$$\Delta\chi^2(\theta)|_{95\%} \leq A; \quad \frac{\int_0^A N d\Delta\chi^2(\theta)}{\int_0^{100} N d\Delta\chi^2(\theta)} = 0.95. \quad (5.2)$$

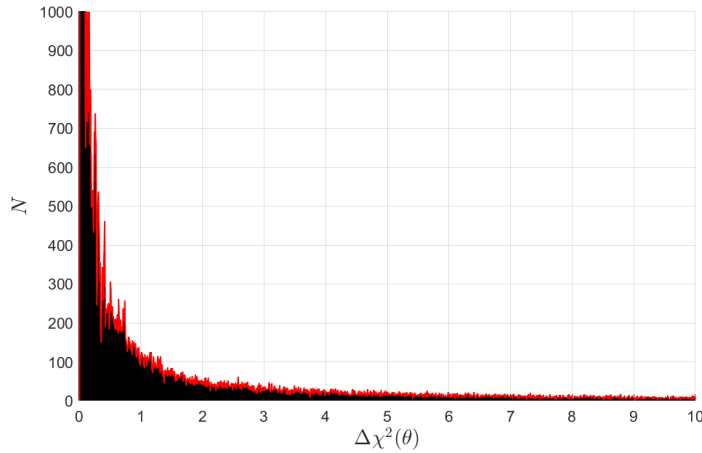


**Figure 5.10:** Distribution of  $\Delta\chi^2(\theta)$  for the scan used to obtain the results in fig. 5.6.



# 6

## Discussion

The results provided in fig. 5.3 and fig. 5.7 indicate a strong, but inverse, resemblance between the constraints set from acquiring acceptable values of the DM relic density and from obtaining the observed CMB power spectrum. This is explained as follows. For a given set of parameter values,  $m_\chi$  and  $m_S$ , such that the evaluated relic density and cross sections are  $(\Omega_\chi h^2)^*$  and  $\langle\sigma v\rangle^*$ , an offset in  $m_S$  such that  $(\Omega_\chi h^2) < (\Omega_\chi h^2)^*$  would imply  $\langle\sigma v\rangle > \langle\sigma v\rangle^*$ , since the relic density is only dependent on  $m_\chi$  and  $\langle\sigma v\rangle$ , as explained in section 3.2.3. This relation is emphasised by comparing the results presented in fig. 5.4 and fig. 5.8. Furthermore, an increase in  $\langle\sigma v\rangle$  would result in an increased energy injection and thus a more distorted CMB power spectrum, as discussed in section 3.2. Thus, the expected "allowed" region will be set by an upper bound  $\Omega_\chi h_0^2 = 0.1188$  and a lower bound  $\Omega_\chi h^2(m_\chi)$ , below which the associated annihilation cross section will obey  $\langle\sigma v\rangle > \langle\sigma v\rangle(m_\chi)$ , where  $\langle\sigma v\rangle(m_\chi)$  is the limit of the excluded region as presented in fig. 5.6. For some  $m_\chi$  it can be seen that  $\Omega_\chi h^2(m_\chi) > \Omega_\chi h_0^2$ , see fig. 5.9, meaning no parameter value  $m_S$  can be chosen such that the point  $(m_\chi, m_S)$  is not excluded from either relic density constraints or CMB constraints. It is further worth noting that for this particular model, the transition between low and high values of the evaluated relic density and subsequently high and low values of the evaluated annihilation cross section occurs very rapidly in the approximate region  $m_S \in (m_\chi, 2m_\chi)$ , see fig. 5.4 and fig. 5.8. Due to this it is a very narrow region in the parameter space that simultaneously could potentially accommodate the conditions required to obtain acceptable values of both the relic density and the annihilation cross section, effectively yielding the inverse resemblance that is observed.

For higher values of  $m_\chi$  it can be seen that there are regions of potentially acceptable values. This appears to be due to the fact that for a fixed value of  $m_\chi$ , the evaluated value of both the relic density and the annihilation cross section are approximately constant for  $m_S \lesssim m_\chi$ , as can be seen from fig. 5.4 and fig. 5.8. This constant value is seen to increase, respectively decrease for higher  $m_\chi$  for the relic density and the cross section respectively. Note that the limit  $\Omega_\chi h^2 = 0.1188$  remains fixed, while the exclusion limit for  $\langle\sigma v\rangle$  increases with increasing  $m_\chi$ , see fig. 5.6 and fig. 5.8. This causes the evaluated cross section to reach values below the exclusion limit before the relic density reaches values above  $\Omega_\chi h^2 = 0.1188$  for low values of  $m_S$ . It can be seen, e.g., fig. 5.4 and fig. 5.8, that the specific values of  $m_\chi$  where the observables cross these limits seem to predominantly depend on the coupling  $\lambda_\chi$ .

It is worth pointing out that at lower masses, the region around the pole  $m_S = 2m_\chi$

is explicitly excluded by CMB data, see fig. 5.7. This is because this region will be more accessible for the interaction between two DM particles and the mediator particle, which is one of the vertices considered in this model. In this region, larger values of the annihilation cross section will therefore be obtained. Since the cross section has a more stringent limit at lower masses, this region is predominantly excluded for lower masses. For higher masses we also expect the pole to be excluded, but since the evaluated cross section needs to be larger for larger masses in order to exclude the region, the region around the pole will become ever narrower for increased masses. Since the resolution of the scans performed in this thesis is very limited, these regions have not been sampled sufficiently for this feature to be visible, if correct. In a similar fashion a very narrow region around the pole can be seen to be allowed when comparing to the observed relic density, see fig. B.2. The reason the region is wider for the CMB results is because the limiting value of the cross section is much lower at these low masses, while the limiting observed relic density remains fixed.

The results obtained in this thesis indicate that the approach of studying the effects of annihilating DM on the CMB power spectrum to set constraints on relevant parameter spaces for specific models is viable and that it may provide valuable, additional constraints to solely studying the relic density. When studying the specific model considered in this thesis it can be seen that combining constraints from CMB and relic density observations, large regions in the parameter space is effectively excluded, and a stringent constraint may be set on the value of  $m_\chi$ . From the results obtained here the allowed values lie approximately in the region  $m_\chi \in (10^2, 10^3)$  GeV, but investigations allowing for varying coupling strengths are needed to set such constraints with confidence. Note that for these results, constraints set by null results from experimental searches have not been included, which would yield even more stringent constraints, most notable for  $m_S$ .

## 6.1 Uncertainties

An issue with obtaining constraints from CMB data is that the scans are very time-consuming and as such it was in this thesis opted to limit the nuisance parameter to a fixed value. From comparing the evaluated excluded region as presented in fig. 5.6 to the results presented in fig. 9 in [2] it does not appear to have caused much, if any, inconsistencies with previously obtained limits. It is however worth mentioning that this may not be the case for other models of energy injection and how this affects the evaluated data should be investigated.

It is also worth mentioning that the results presented in this thesis are limited to three different sets of coupling constants. This is because when attempting to perform scans in parameter spaces that were larger than 2-dimensional, the scans took exponentially longer time and often got stuck in local minima, from which they could not continue. The options were then either to focus on few discrete sets of parameter values at which larger regions in the subspace  $(m_\chi, m_S)$  could be sampled, or limit to very small regions in higher-dimensional parameter spaces. The first option was

deemed preferable, as the results obtained would provide more information of the DM model at hand.

As mentioned in section 3.2.3, it is possible that the considered DM particle does not constitute all of the DM. Although easily implemented for the relic density constraints, its effect on the CMB constraints are not as easily accounted for. If this DM species does not account for all the DM, the injected energy in the early Universe will be less than what is here assumed, see eq. (3.23), and the constraints set by the CMB power spectrum will be less stringent than here presented.

In evaluating the rate of energy deposition, the efficiency function for annihilating DM was evaluated as expressed in eq. (3.22). The transition function that appears in this calculation depends on the free electron fraction, and the implemented transition function implicitly assumes the evolution of the free electron fraction is identical to the evolution in the absence of energy injection [2]. This assumption will in general lead to an underestimation of the impact on the CMB [2], which may have affected the results presented in this thesis.

## 6.2 Further development

For further investigations using this approach there are several potential areas of interest that could be focused on. The first and probably most significant extension to be made on this general approach for setting constraints on the model parameters is to include more fermionic final states. In order to do this, specific forms of energy injection to the primordial plasma must be described for the additional final states. Another investigation of further interest would be to apply this approach to different DM models, which could be incorporated with relative ease by implementing different Lagrangians in the original model. If only considering the  $e^+e^-$  final state, the implementation presented in this thesis can be directly implemented with the only modification required being to the original model file implemented in FeynRules as described in appendix A.3.2.



# 7

## Conclusions

In this thesis, the possibility to study the effects of energy injection from annihilating DM on the observed CMB power spectrum to constrain DM model parameters has been investigated. A specific DM model consisting of a vectorial (spin 1) DM and a scalar (spin 0) mediator particle which interacts with the SM states has been investigated, in particular considering  $e^+e^-$  final states. Excluded regions in the subspace of the DM and mediator masses have been identified for three sets of coupling strengths, and when including constraints set by the observed relic density, it is shown that the specific model investigated is largely excluded, apart from a narrow region of values of the DM mass;  $m_\chi \in (\sim 10^2, \sim 10^3)$  GeV. It is thus concluded that using the CMB power spectrum to constrain DM model parameters is viable and may provide additional constraints to previously studied relic density constraints.

This study could be continued to investigate broader regions in the investigated parameter spaces, along with other models, possibly including other final states, to further constrain such models. Achieving credible and stringent constraints of various DM models could ultimately be used to guide the planning and execution of next-generation DM searches.



# Bibliography

- [1] Gianfranco Bertone and Dan Hooper. “History of dark matter”. In: *Reviews of Modern Physics* 90.4 (Oct. 2018). ISSN: 1539-0756. DOI: 10.1103/revmodphys.90.045002. URL: <http://dx.doi.org/10.1103/RevModPhys.90.045002>.
- [2] Janina J. Renk et al. “CosmoBit: a GAMBIT module for computing cosmological observables and likelihoods”. In: *Journal of Cosmology and Astroparticle Physics* 2021.02 (Feb. 2021), pp. 022–022. ISSN: 1475-7516. DOI: 10.1088/1475-7516/2021/02/022. URL: <http://dx.doi.org/10.1088/1475-7516/2021/02/022>.
- [3] Heinz Andernach and Fritz Zwicky. *English and Spanish Translation of Zwicky’s (1933) The Redshift of Extragalactic Nebulae*. 2017. arXiv: 1711.01693 [astro-ph.IM].
- [4] J. L. Russell. “Kepler’s Laws of Planetary Motion: 1609-1666”. In: *The British Journal for the History of Science* 2.1 (1964), pp. 1–24. ISSN: 00070874, 1474001X. URL: <http://www.jstor.org/stable/4025081>.
- [5] Richard S. Ellis. “Gravitational lensing: a unique probe of dark matter and dark energy”. In: *Philosophical Transactions of the Royal Society A: Mathematical, Physical and Engineering Sciences* 368.1914 (2010), pp. 967–987. DOI: 10.1098/rsta.2009.0209. eprint: <https://royalsocietypublishing.org/doi/pdf/10.1098/rsta.2009.0209>. URL: <https://royalsocietypublishing.org/doi/abs/10.1098/rsta.2009.0209>.
- [6] D. J. Fixsen. “THE TEMPERATURE OF THE COSMIC MICROWAVE BACKGROUND”. In: *The Astrophysical Journal* 707.2 (Nov. 2009), pp. 916–920. ISSN: 1538-4357. DOI: 10.1088/0004-637x/707/2/916. URL: <http://dx.doi.org/10.1088/0004-637x/707/2/916>.
- [7] Suzanne Staggs, Jo Dunkley, and Lyman Page. “Recent discoveries from the cosmic microwave background: a review of recent progress”. In: *Reports on Progress in Physics* 81.4 (2018), p. 044901.
- [8] N. Aghanim et al. “Planck 2018 results”. In: *Astronomy & Astrophysics* 641 (Sept. 2020), A6. ISSN: 1432-0746. DOI: 10.1051/0004-6361/201833910. URL: <http://dx.doi.org/10.1051/0004-6361/201833910>.

- [9] E. Aprile et al. “First axion results from the XENON100 experiment”. In: *Physical Review D* 90.6 (Sept. 2014). ISSN: 1550-2368. DOI: 10.1103/physrevd.90.062009. URL: <http://dx.doi.org/10.1103/PhysRevD.90.062009>.
- [10] P. Agnes et al. “First results from the DarkSide-50 dark matter experiment at Laboratori Nazionali del Gran Sasso”. In: *Physics Letters B* 743 (Apr. 2015), pp. 456–466. ISSN: 0370-2693. DOI: 10.1016/j.physletb.2015.03.012. URL: <http://dx.doi.org/10.1016/j.physletb.2015.03.012>.
- [11] C. Amole et al. “Dark matter search results from the PICO-60CF3Ibubble chamber”. In: *Physical Review D* 93.5 (Mar. 2016). ISSN: 2470-0029. DOI: 10.1103/physrevd.93.052014. URL: <http://dx.doi.org/10.1103/PhysRevD.93.052014>.
- [12] G. Angloher et al. “Results on light dark matter particles with a low-threshold CRESST-II detector”. In: *The European Physical Journal C* 76.1 (Jan. 2016). ISSN: 1434-6052. DOI: 10.1140/epjc/s10052-016-3877-3. URL: <http://dx.doi.org/10.1140/epjc/s10052-016-3877-3>.
- [13] D. S. Akerib et al. “Results from a Search for Dark Matter in the Complete LUX Exposure”. In: *Physical Review Letters* 118.2 (Jan. 2017). ISSN: 1079-7114. DOI: 10.1103/physrevlett.118.021303. URL: <http://dx.doi.org/10.1103/PhysRevLett.118.021303>.
- [14] E. Armengaud et al. “Constraints on low-mass WIMPs from the EDELWEISS-III dark matter search”. In: *Journal of Cosmology and Astroparticle Physics* 2016.05 (May 2016), pp. 019–019. ISSN: 1475-7516. DOI: 10.1088/1475-7516/2016/05/019. URL: <http://dx.doi.org/10.1088/1475-7516/2016/05/019>.
- [15] Giorgio Arcadi et al. “The waning of the WIMP? A review of models, searches, and constraints”. In: *The European Physical Journal C* 78.3 (Mar. 2018). ISSN: 1434-6052. DOI: 10.1140/epjc/s10052-018-5662-y. URL: <http://dx.doi.org/10.1140/epjc/s10052-018-5662-y>.
- [16] Rebecca K. Leane et al. “Celestial-body focused dark matter annihilation throughout the Galaxy”. In: *Physical Review D* 103.7 (Apr. 2021). ISSN: 2470-0029. DOI: 10.1103/physrevd.103.075030. URL: <http://dx.doi.org/10.1103/PhysRevD.103.075030>.
- [17] Raghuveer Garani, Aritra Gupta, and Nirmal Raj. “Observing the thermalization of dark matter in neutron stars”. In: *Physical Review D* 103.4 (Feb. 2021). ISSN: 2470-0029. DOI: 10.1103/physrevd.103.043019. URL: <http://dx.doi.org/10.1103/PhysRevD.103.043019>.
- [18] Christian Gross, Oleg Lebedev, and Yann Mambrini. *Non-Abelian gauge fields as dark matter*. 2015. arXiv: 1505.07480 [hep-ph].



- 
- [19] Yeinzon Rodriguez. *A New Pedagogical Way of Finding Out the Gauge Field Strength Tensor in Abelian and Non-Abelian Local Gauge Field Theories*. 2016. arXiv: 1512.03827 [physics.gen-ph].
- [20] Andrej B. Arbuzov, Lukasz A. Glinka, and Victor N. Pervushin. *Classical Scalar Field Potential in the Standard Model*. 2008. arXiv: 0805.3075 [hep-ph].
- [21] N Beisert. “Quantum Field Theory I”. In: *ETH Zurich, HS12* (2012).
- [22] Adam Alloul et al. “FeynRules 2.0 — A complete toolbox for tree-level phenomenology”. In: *Computer Physics Communications* 185.8 (Aug. 2014), pp. 2250–2300. ISSN: 0010-4655. DOI: 10.1016/j.cpc.2014.04.012. URL: <http://dx.doi.org/10.1016/j.cpc.2014.04.012>.
- [23] G. Bélanger et al. “micrOMEGAs: A program for calculating the relic density in the MSSM”. In: *Computer Physics Communications* 149.2 (Dec. 2002), pp. 103–120. ISSN: 0010-4655. DOI: 10.1016/S0010-4655(02)00596-9. URL: [http://dx.doi.org/10.1016/S0010-4655\(02\)00596-9](http://dx.doi.org/10.1016/S0010-4655(02)00596-9).
- [24] G. Bélanger et al. “micrOMEGAs\_3: A program for calculating dark matter observables”. In: *Computer Physics Communications* 185.3 (Mar. 2014), pp. 960–985. ISSN: 0010-4655. DOI: 10.1016/j.cpc.2013.10.016. URL: <http://dx.doi.org/10.1016/j.cpc.2013.10.016>.
- [25] Silvia Galli et al. “CMB constraints on dark matter models with large annihilation cross section”. In: *Physical Review D* 80.2 (July 2009). ISSN: 1550-2368. DOI: 10.1103/physrevd.80.023505. URL: <http://dx.doi.org/10.1103/PhysRevD.80.023505>.
- [26] Julien Lesgourgues. *The Cosmic Linear Anisotropy Solving System (CLASS) I: Overview*. 2011. arXiv: 1104.2932 [astro-ph.IM].
- [27] Julien Lesgourgues and Thomas Tram. “Fast and accurate CMB computations in non-flat FLRW universes”. In: *Journal of Cosmology and Astroparticle Physics* 2014.09 (Sept. 2014), pp. 032–032. ISSN: 1475-7516. DOI: 10.1088/1475-7516/2014/09/032. URL: <http://dx.doi.org/10.1088/1475-7516/2014/09/032>.
- [28] Mihailo Backović, Kyoungchul Kong, and Mathew McCaskey. “MadDM v.1.0: Computation of dark matter relic abundance using MadGraph 5”. In: *Physics of the Dark Universe* 5-6 (Dec. 2014), pp. 18–28. ISSN: 2212-6864. DOI: 10.1016/j.dark.2014.04.001. URL: <http://dx.doi.org/10.1016/j.dark.2014.04.001>.
- [29] P. A. R. Ade et al. “Planck 2015 results”. In: *Astronomy & Astrophysics* 594 (Sept. 2016), A13. ISSN: 1432-0746. DOI: 10.1051/0004-6361/201525830. URL: <http://dx.doi.org/10.1051/0004-6361/201525830>.
- [30] Torsten Bringmann et al. “Precise dark matter relic abundance in decoupled sectors”. In: *Physics Letters B* 817 (June 2021), p. 136341. ISSN: 0370-2693.

- DOI: 10.1016/j.physletb.2021.136341. URL: <http://dx.doi.org/10.1016/j.physletb.2021.136341>.
- [31] Patrick Royston. “Profile likelihood for estimation and confidence intervals”. In: *The Stata Journal* 7.3 (2007), pp. 376–387.
- [32] Torsten Bringmann et al. “DarkBit: a GAMBIT module for computing dark matter observables and likelihoods”. In: *The European Physical Journal C* 77.12 (Dec. 2017). ISSN: 1434-6052. DOI: 10.1140/epjc/s10052-017-5155-4. URL: <http://dx.doi.org/10.1140/epjc/s10052-017-5155-4>.
- [33] N. Aghanim et al. “Planck 2018 results”. In: *Astronomy & Astrophysics* 641 (Sept. 2020), A5. ISSN: 1432-0746. DOI: 10.1051/0004-6361/201936386. URL: <http://dx.doi.org/10.1051/0004-6361/201936386>.
- [34] Gregory D. Martinez et al. “Comparison of statistical sampling methods with ScannerBit, the GAMBIT scanning module”. In: *The European Physical Journal C* 77.11 (Nov. 2017). ISSN: 1434-6052. DOI: 10.1140/epjc/s10052-017-5274-y. URL: <http://dx.doi.org/10.1140/epjc/s10052-017-5274-y>.
- [35] Peter Athron et al. “GAMBIT: the global and modular beyond-the-standard-model inference tool”. In: *The European Physical Journal C* 77.11 (Nov. 2017). ISSN: 1434-6052. DOI: 10.1140/epjc/s10052-017-5321-8. URL: <http://dx.doi.org/10.1140/epjc/s10052-017-5321-8>.
- [36] Alexander Belyaev, Neil D. Christensen, and Alexander Pukhov. “CalcHEP 3.4 for collider physics within and beyond the Standard Model”. In: *Computer Physics Communications* 184.7 (July 2013), pp. 1729–1769. ISSN: 0010-4655. DOI: 10.1016/j.cpc.2013.01.014. URL: <http://dx.doi.org/10.1016/j.cpc.2013.01.014>.
- [37] A. Arbey. “AlterBBN: A program for calculating the BBN abundances of the elements in alternative cosmologies”. In: *Computer Physics Communications* 183.8 (Aug. 2012), pp. 1822–1831. ISSN: 0010-4655. DOI: 10.1016/j.cpc.2012.03.018. URL: <http://dx.doi.org/10.1016/j.cpc.2012.03.018>.
- [38] Diego Blas, Julien Lesgourgues, and Thomas Tram. “The Cosmic Linear Anisotropy Solving System (CLASS). Part II: Approximation schemes”. In: *Journal of Cosmology and Astroparticle Physics* 2011.07 (July 2011), pp. 034–034. ISSN: 1475-7516. DOI: 10.1088/1475-7516/2011/07/034. URL: <http://dx.doi.org/10.1088/1475-7516/2011/07/034>.
- [39] Benjamin Audren et al. “Conservative constraints on early cosmology with MONTEPYTHON”. In: *Journal of Cosmology and Astroparticle Physics* 2013.02 (Feb. 2013), pp. 001–001. ISSN: 1475-7516. DOI: 10.1088/1475-7516/2013/02/001. URL: <http://dx.doi.org/10.1088/1475-7516/2013/02/001>.
- [40] Thejs Brinckmann and Julien Lesgourgues. *MontePython 3: boosted MCMC sampler and other features*. 2018. arXiv: 1804.07261 [astro-ph.CO].

- [41] Michael J. Mortonson, Hiranya V. Peiris, and Richard Easther. “Bayesian analysis of inflation: Parameter estimation for single field models”. In: *Physical Review D* 83.4 (Feb. 2011). ISSN: 1550-2368. DOI: 10.1103/physrevd.83.043505. URL: <http://dx.doi.org/10.1103/PhysRevD.83.043505>.
- [42] Richard Easther and Hiranya V. Peiris. “Bayesian analysis of inflation. II. Model selection and constraints on reheating”. In: *Physical Review D* 85.10 (May 2012). ISSN: 1550-2368. DOI: 10.1103/physrevd.85.103533. URL: <http://dx.doi.org/10.1103/PhysRevD.85.103533>.
- [43] Layne C. Price et al. “MULTIMODECODE: an efficient numerical solver for multifield inflation”. In: *Journal of Cosmology and Astroparticle Physics* 2015.03 (Mar. 2015), pp. 005–005. ISSN: 1475-7516. DOI: 10.1088/1475-7516/2015/03/005. URL: <http://dx.doi.org/10.1088/1475-7516/2015/03/005>.
- [44] P. A. R. Ade et al. “Planck intermediate results”. In: *Astronomy & Astrophysics* 566 (June 2014), A54. ISSN: 1432-0746. DOI: 10.1051/0004-6361/201323003. URL: <http://dx.doi.org/10.1051/0004-6361/201323003>.



# A

## Implementation

### A.1 Modifying GAMBIT

In this chapter the implemented code is carefully detailed.

#### A.1.1 Defining the model AnnihilatingDM\_Thesis

```
#define MODEL AnnihilatingDM_Thesis
void MODEL_NAMESPACE::
    AnnihilatingDM_Thesis_to_AnnihilatingDM_general (const
        ModelParameters &myP, ModelParameters &targetP)
{
    logger() << "Running interpret_as_parent calculations for
    AnnihilatingDM_Thesis --> AnnihilatingDM_general ..." << LogTags::
        info << EOM;

    double m_DM = myP.getValue("mass_DM");
    double m_med = myP.getValue("mass_med");
    double lambda_DM = myP.getValue("lambda_DM");
    double lambda_med_ferm = myP.getValue("lambda_med_ferm");
    double lambda_med = myP.getValue("lambda_med");
    int version = myP.getValue("version");

    targetP.setValue("mass", m_DM);
    targetP.setValue("sigmav", CalculateSigmaV(m_DM, m_med, lambda_DM,
        lambda_med_ferm, lambda_med, version));
}
#undef MODEL
```

#### A.1.2 Defining the local function CalculateSigmaV

```
// Add this at the top of the code if not already present

#include <thread>
#include <string>
#include <vector>
#include <fstream>
#include <stdio.h>
#include <stdlib.h>
#include <sched.h>
#include <string.h>
#include <math.h>
#define DEST_SIZE 200
```

```
double CalculateSigmaV(double m_DM, double m_med, double lambda_DM,
    double lambda_med_ferm, double lambda_med, int version){

    double sigmaV;

    // This will be used to specify the file

    char snum[20];
    sprintf(snum, "%.4f", m_DM);

    // collect temporary folder path
    std::string TMPDIR = getenv("TMPDIR");

    // make the parameter file to be used for MicrOmegas

    char dest_1[DEST_SIZE];
    strcpy(dest_1, TMPDIR.c_str());
    strcat(dest_1, "/data_");
    strcat(dest_1, snum);
    strcat(dest_1, ".par");

    // This line will run MicrOmegas
    char dest_2[DEST_SIZE] = "Backends/installed/micromegas
        /3.6.9.2/";
    if (version == 1){
        strcat(dest_2, "Spin0/sigmav ");
    }
    else{
        strcat(dest_2, "Validation0/sigmav ");
    }
    strcat(dest_2, dest_1);

    // This line will remove the parameter file dest_1
    char dest_3[DEST_SIZE] = "rm -rf ";
    strcat(dest_3, dest_1);

    // This is the address to the parameter file we want to
    read off
    char dest_4[DEST_SIZE];
    strcpy(dest_4, TMPDIR.c_str());
    strcat(dest_4, "/sigmasave_");
    strcat(dest_4, snum);
    strcat(dest_4, ".txt");

    // This is the line used to delete file dest_4
    char dest_5[DEST_SIZE] = "rm -rf ";
    strcat(dest_5, dest_4);

    // Print the current variables to an external file, needed
    to run micrOmega later

    FILE * fPtr;
    fPtr = fopen(dest_1, "w");

    if (fPtr!=NULL)
```

```

{
    // write to parameter file to be used for MicroMegas
    fprintf(fPtr, "Mchi %.4f\n", m_DM);
    fprintf(fPtr, "MYO %.4f\n", m_med);
    fprintf(fPtr, "lDM %.4f\n", lambda_DM);
    fprintf(fPtr, "lmedferm %.4f\n", lambda_med_ferm);
    fprintf(fPtr, "lmed %.4f\n", lambda_med);

    fclose(fPtr);

    // Run the model to evaluate sigmaV

    system(dest_2);

    // remove the parameter file

    system(dest_3);

    // Collect the value of sigmaV saved to an external file
    from micrOmega

    int N = 8; // number of decimal places
    int total = N+7;
    char str[total];

    FILE * sigmaread;
    sigmaread = fopen(dest_4, "r");
    if (sigmaread!=NULL)
    {
        if( fgets (str, total, sigmaread)!=NULL ) {

            puts(str);
            sigmaV = atof(str);
            fclose(sigmaread);

            // Keep the code from crashing by returning bad values
            instead of 0

            if (sigmaV == 0.0) {
                sigmaV = 1000000.0;
            }
        }
        else {
            sigmaV = 1000000.0;
        }
    }
    else {
        sigmaV = 1000000.0;
    }

    // remove the sigma file

    system(dest_5);

}
else{

```

```

        sigmaV = 1000000.0;
    }
    return sigmaV;
}

```

### A.1.3 Declaring the model AnnihilatingDM\_Thesis

```

#define MODEL AnnihilatingDM_Thesis
#define PARENT AnnihilatingDM_general
START_MODEL
DEFINEPARS(mass_DM) // Mass of dark matter candidate [GeV]
DEFINEPARS(mass_med) // Mass of mediator candidate [GeV]
DEFINEPARS(lambda_DM) // Coupling strength related to X.S.S and X
.X.S.S
DEFINEPARS(lambda_med_ferm) // Coupling strength of S.e+.e-
DEFINEPARS(lambda_med) // Coupling strength of S.S.S
DEFINEPARS(version) // Selects what version of the code that
should be executed

INTERPRET_AS_PARENT_FUNCTION(
    AnnihilatingDM_Thesis_to_AnnihilatingDM_general)
#undef PARENT
#undef MODEL

```

### A.1.4 Defining the function energy\_injection...

```

void energy_injection_spectrum_AnnihilatingDM_Thesis(DarkAges::
    Energy_injection_spectrum& spectrum)
{
    using namespace Pipes::
        energy_injection_spectrum_AnnihilatingDM_Thesis;

    // We now only assume energy injection through electrons/
    positrons

    double m = *Param["mass_DM"];

    double BR_el = 1.0;
    double BR_ph = 0.0;

    logger() << LogTags::debug << "Creating \'
        energy_injection_spectrum\' for \'AnnihilatingDM_Thesis\'\'
        n\n";
    logger() << "- Branching fraction into e+/e-: " << BR_el;
    logger() << "\n- Branching fraction into photons: " << BR_ph;
    logger() << "\n- Branching fraction into inefficient final
        state: " << 1 - BR_ph - BR_el << "\n" << EOM;

    if (m <= m_electron && BR_el >= std::numeric_limits<double>::
        epsilon())
    {
        std::ostream err;
        err << "The mass of the annihilating dark matter candidate
            is below the electron mass.";
    }
}

```



```

    err << " No production of e+/e- is possible.";
    model_error().raise(LOCAL_INFO,err.str());
}

spectrum.E_el.clear();
spectrum.E_ph.clear();
spectrum.spec_el.clear();
spectrum.spec_ph.clear();

spectrum.E_el.resize(1,std::max(m-m_electron, std::
    numeric_limits<double>::min()));
spectrum.E_ph.resize(1,m);
spectrum.spec_el.resize(1,BR_el*2e9);
spectrum.spec_ph.resize(1,BR_ph*2e9);
}

```

### A.1.5 Declaring the function energy\_injection...

```

#define FUNCTION energy_injection_spectrum_AnnihilatingDM_Thesis
    START_FUNCTION(DarkAges::Energy_injection_spectrum)
    ALLOW_MODEL(AnnihilatingDM_Thesis)
#undef FUNCTION

```

### A.1.6 Defining the functions RD\_oh2\_Thesis and CalculateOmega

The function that returns the evaluated relic density is RD\_oh2\_Thesis, but the evaluation takes place in another function, CalculateOmega. Both functions are written in the same file as shown below.

```

void RD_oh2_Thesis(double &result)
{
    using namespace Pipes::RD_oh2_Thesis;
    double m_DM = *Param["mass_DM"];
    double m_med = *Param["mass_med"];
    double lambda_DM = *Param["lambda_DM"];
    double lambda_med_ferm = *Param["lambda_med_ferm"];
    double lambda_med = *Param["lambda_med"];
    int version = *Param["version"];

    result = CalculateOmega(m_DM, m_med, lambda_DM,
        lambda_med_ferm, lambda_med, version);
}

// Add this at the top of the code if not already present

#include <thread>
#include <string>
#include <vector>
#include <fstream>
#include <stdio.h>
#include <stdlib.h>
#include <sched.h>
#include <string.h>
#include <math.h>
#define DEST_SIZE 200

```

```
double CalculateOmega(double m_DM, double m_med, double
    lambda_DM, double lambda_med_ferm, double lambda_med, int
    version){

    double Omega;

    // This will be used to specify the file

    char snum[20];
    sprintf(snum, "%.4f", m_DM);

    // collect temporary folder path
    std::string TMPDIR = getenv("TMPDIR");

    // make the parameter file to be used for MicrOmegas

    char dest_1[DEST_SIZE];
    strcpy(dest_1, TMPDIR.c_str());
    strcat(dest_1, "/data_");
    strcat(dest_1, snum);
    strcat(dest_1, ".par");

    // This line will run MicrOmegas
    char dest_2[DEST_SIZE] = "Backends/installed/micromegas
        /3.6.9.2/";
    if (version == 1){
        strcat(dest_2, "Spin0/omega ");
    }
    else{
        strcat(dest_2, "Validation0/omega ");
    }
    strcat(dest_2, dest_1);

    // This line will remove the parameter file dest_1
    char dest_3[DEST_SIZE] = "rm -rf ";
    strcat(dest_3, dest_1);

    // This is the address to the parameter file we want to
    read off
    char dest_4[DEST_SIZE];
    strcpy(dest_4, TMPDIR.c_str());
    strcat(dest_4, "/omegasave_");
    strcat(dest_4, snum);
    strcat(dest_4, ".txt");

    // This is the line used to delete file dest_4
    char dest_5[DEST_SIZE] = "rm -rf ";
    strcat(dest_5, dest_4);

    // Print the current variables to an external file, needed
    to run micrOmega later

    FILE * fPtr;
    fPtr = fopen(dest_1, "w");
```

```

if (fPtr!=NULL)
{

    fprintf(fPtr, "Mchi %.4f\n", m_DM);
    fprintf(fPtr, "MYO %.4f\n", m_med);
    fprintf(fPtr, "lDM %.4f\n", lambda_DM);
    fprintf(fPtr, "lmedferm %.4f\n", lambda_med_ferm);
    fprintf(fPtr, "lmed %.4f\n", lambda_med);

    fclose(fPtr);

// Run the model to evaluate Omega

system(dest_2);

// remove the parameter file

system(dest_3);

// Collect the value of omega saved to an external file
    from micrOmega

int N = 8; // number of decimal places
int total = N+7;
char str[total];

FILE * omegaread;
omegaread = fopen(dest_4, "r");
if (omegaread!=NULL)
{
    if( fgets (str, total, omegaread)!=NULL ) {

        puts(str);
        Omega = atof(str);
        fclose(omegaread);

        if (Omega < 0.0) {
            Omega = 1.E20;
        }

    }
    else {
        Omega = 1.E20;
    }
}
else {
    Omega = 1.E20;
}

// remove the omega file

system(dest_5);
}
else{
    Omega = 1.E20;
}

```

```

    }

    return Omega;
}

```

### A.1.7 Declaring the function RD\_oh2\_Thesis

```

#define FUNCTION RD_oh2_Thesis
    START_FUNCTION(double)
    ALLOW_MODEL_DEPENDENCE(AnnihilatingDM_Thesis)
#undef FUNCTION

```

### A.1.8 Additional functions to save parameters

```

void function_sigmap(double& result)
{
    using namespace Pipes::function_sigmap;
    double m_DM = *Param["mass_DM"];
    double m_med = *Param["mass_med"];
    double lambda_DM = *Param["lambda_DM"];
    double lambda_med_ferm = *Param["lambda_med_ferm"];
    double lambda_med = *Param["lambda_med"];
    int version = *Param["version"];

    double new_sigmap = CalculateSigmap(m_DM, m_med, lambda_DM,
        lambda_med_ferm, lambda_med, version);

    printf("--- I save sigmap to be %.8E[cm^3/s]\n", new_sigmap);
    result = new_sigmap;
}

void function_oh2(double &result)
{
    using namespace Pipes::function_oh2;
    double m_DM = *Param["mass_DM"];
    double m_med = *Param["mass_med"];
    double lambda_DM = *Param["lambda_DM"];
    double lambda_med_ferm = *Param["lambda_med_ferm"];
    double lambda_med = *Param["lambda_med"];
    int version = *Param["version"];

    double Omega = CalculateOmega(m_DM, m_med, lambda_DM,
        lambda_med_ferm, lambda_med, version);

    printf("--- I save Omega to be %.8E[cm^3/s]\n", Omega);
    result = Omega;
}

```

### A.1.9 Declaring parameter functions

```
#define CAPABILITY capability_for_sigmap
START_CAPABILITY
#define FUNCTION function_sigmap
START_FUNCTION(double)
ALLOW_MODELS(AnnihilatingDM_Thesis)
#undef FUNCTION
#undef CAPABILITY

#define CAPABILITY capability_for_omega
START_CAPABILITY
#define FUNCTION function_oh2
START_FUNCTION(double)
ALLOW_MODELS(AnnihilatingDM_Thesis)
#undef FUNCTION
#undef CAPABILITY
```

## A.2 Modifying micrOMEGAs

### A.2.1 Calculating the relic density

```
#include "../sources/micromegas.h"
#include "../sources/micromegas_aux.h"
#include "lib/pmodel.h"

#include <stdio.h>
#include <stdlib.h>
#include <sched.h>
#include <string.h>

#define OMEGA
#define DEST_SIZE 200

int main(int argc, char** argv)
{
    int err;
    char cdmName[10];
    int spin2, charge3, cdim;

    ForceUG=0; /* to Force Unitary Gauge assign 1 */

    if(argc==1)
    {
        printf(" Correct usage: ./main <file with parameters> \n");
        printf("Example: ./main data1.par\n");
        exit(1);
    }

    err=readVar(argv[1]);

    if(err==-1) {printf("Can not open the file\n"); exit(1);}
    else if(err>0) { printf("Wrong file contents at line %d\n",err);
        exit(1);}
}
```

```

err=sortOddParticles(cdmName);
if(err) { printf("Can't calculate %s\n",cdmName); return 1;}

qNumbers(cdmName, &spin2, &charge3, &cdim);
/*printf("\nDark matter candidate is '%s' with spin=%d/2\n",
    cdmName, spin2); */
if(charge3) { printf("Dark Matter has electric charge %d*3\n",
    charge3); exit(1);}
if(cdim!=1) { printf("Dark Matter ia a color particle\n"); exit
    (1);}

#ifdef OMEGA
{ int fast=1;
  double Beps=1.E-5, cut=0.01;
  double Omega,Xf;

  // to exclude processes with virtual W/Z in DM annihilation
  VZdecay=0; VWdecay=0; cleanDecayTable();

  // to include processes with virtual W/Z also in co-annihilation
  // VZdecay=2; VWdecay=2; cleanDecayTable();

  printf("\n=== Calculation of relic density ===\n");
  char snum[20];

  sprintf(snum, "%.4f", Mcdm);

  char* dest = getenv("TMPDIR");
  strcat(dest, "/omegasave_");
  strcat(dest, snum);
  strcat(dest, ".txt");

  Omega=darkOmega(&Xf,fast,Beps);

  printf("Xf=%.2e Omega=%.2e\n",Xf,Omega);
  FILE *fp;
  fp = fopen(dest, "w");
  if (fp!=NULL)
  {
    fprintf(fp, "%.8E", Omega);
    fclose(fp);
  }
}
#endif

killPlots();
return 0;
}

```

## A.2.2 Calculating the cross section

```

#include "../sources/micromegas.h"
#include "../sources/micromegas_aux.h"
#include "lib/pmodel.h"

```

```

#include <stdio.h>
#include <stdlib.h>
#include <sched.h>
#include <string.h>

#define INDIRECT_DETECTION
#define DEST_SIZE 200

int main(int argc, char** argv)
{
    int err;
    char cdmName[10];
    int spin2, charge3, cdim;

    ForceUG=0; /* to Force Unitary Gauge assign 1 */

    if(argc==1)
    {
        printf(" Correct usage: ./main <file with parameters> \n");
        printf("Example: ./main data1.par\n");
        exit(1);
    }

    err=readVar(argv[1]);

    if(err==-1) {printf("Can not open the file\n"); exit(1);}
    else if(err>0) { printf("Wrong file contents at line %d\n",err);
        exit(1);}

    err=sortOddParticles(cdmName);
    if(err) { printf("Can't calculate %s\n",cdmName); return 1;}

    qNumbers(cdmName, &spin2, &charge3, &cdim);
    printf("\nDark matter candidate is '%s' with spin=%d/2\n",
        cdmName, spin2);
    if(charge3) { printf("Dark Matter has electric charge %d*3\n",
        charge3); exit(1);}
    if(cdim!=1) { printf("Dark Matter ia a color particle\n"); exit
        (1);}

#ifdef INDIRECT_DETECTION
{
    int fast=1;
    double Beps=1.E-5, cut=0.01;
    int err,i;
    double sigmaV;

    char snum[20];

    sprintf(snum, "%.4f", Mcdm);

    char* dest = getenv("TMPDIR");
    strcat(dest, "/sigmasave_");
    strcat(dest, snum);
    strcat(dest, ".txt");

    double Xf;

```

```

double Omega=darkOmega(&Xf,fast,Beps);

if (Xf == 0){
    sigmaV = 1E-10;
}
else
{
    double pbccm = 2.99792458E-26;
    sigmaV = pbccm*vSigma(Mcdm/Xf,Beps,fast);
}

printf("\n=== Indirect detection =====\n");

printf("sigmav=%.2E[cm^3/s]\n",sigmaV);
FILE *fp;
fp = fopen(dest, "w");
if (fp!=NULL)
{
    fprintf(fp, "%.8E", sigmaV);
    fclose(fp);
}

}
#endif

killPlots();
return 0;
}

```

## A.3 Implementing the Lagrangian

### A.3.1 Model file

```

(* ***** *)
(* **** Particle classes **** *)
(* ***** *)
M$ClassesDescription = {

(* New particles *)

(* DM *)
V[21] == {
    ClassName -> chi,
    SelfConjugate -> True,
    Mass -> {Mchi, 1000.},
    Width -> 0,
    ParticleName -> "~chi"
},

(* Mediator *)
S[21] == {

```



```

        ClassName -> Y0,
        SelfConjugate -> True,
        Mass -> {MY0, 1000.},
        Width -> 0,
        ParticleName -> "Y0",
        PDG -> 1000
    },
.
.
.

(* ***** *)
(* ***** Parameters ***** *)
(* ***** *)
M$Parameters = {

    (* New parameters *)

    lDM == {
        ParameterType -> External,
        BlockName -> DMINPUTS,
        OrderBlock -> 1,
        Value -> 1.0,
        InteractionOrder -> {QED, -2},
        Description -> "Coupling between dark matter and mediator"
    },

    lmedferm == {
        ParameterType -> External,
        BlockName -> DMINPUTS,
        OrderBlock -> 2,
        Value -> 1.0,
        InteractionOrder -> {QED, -2},
        Description -> "Self-coupling of mediator"
    },

    lmed == {
        ParameterType -> External,
        BlockName -> DMINPUTS,
        OrderBlock -> 3,
        Value -> 1.0,
        InteractionOrder -> {QED, -2},
        Description -> "Coupling between mediator and electron-
            positron pair"
    },
.
.
.

(* ***** *)
(* ***** Lagrangian ***** *)
(* ***** *)

```

```
(* New Lagrangian *)

LDarkMatter := Block[{mu},
  ExpandIndices[lDM/2 Mchi chi[mu] chi[mu] Y0 + lDM lDM/8 chi[mu]
    chi[mu] Y0 Y0 + lmedferm/Sqrt[2] Me/vev Y0 ebar.e - lmed/6 MY0
    Y0 Y0 Y0]];

LDarkMatterValidation := Block[{mu},
  ExpandIndices[lDM/2 Mchi chi[mu] chi[mu] Y0 + lDM lDM/8 chi[mu]
    chi[mu] Y0 Y0 + lmedferm/Sqrt[2] Me/vev Y0 ebar.e + lmedferm/
    Sqrt[2] MMU/vev Y0 mubar.mu + lmedferm/Sqrt[2] MTA/vev Y0
    tabar.ta + lmedferm/Sqrt[2] MU/vev Y0 ubar.u + lmedferm/Sqrt
    [2] MC/vev Y0 cbar.c + lmedferm/Sqrt[2] MT/vev Y0 tbar.t +
    lmedferm/Sqrt[2] MD/vev Y0 dbar.d + lmedferm/Sqrt[2] MS/vev Y0
    sbar.s + lmedferm/Sqrt[2] MB/vev Y0 bbar.b - lmed/6 MY0 Y0 Y0
    Y0]];

.
.
.
```

### A.3.2 Expanding the Lagrangian

```
Quit[]

$FeynRulesPath = SetDirectory["~/feynrules-current"]
<< FeynRules`
SetDirectory[$FeynRulesPath <> "/Models/SM"]
LoadModel["SM.fr"]
SetDirectory["~/gambit/Backends/installed/micromegas/3.6.9.2/Spin0/
work"]
FeynmanGauge = True
WriteCHOutput[LDarkMatter, Output -> "models"];

$FeynRulesPath =
  SetDirectory["~/feynrules-current"]
<< FeynRules`
SetDirectory[$FeynRulesPath <> "/Models/SM"]
LoadModel["SM.fr"]
SetDirectory["~/gambit/Backends/installed/micromegas/3.6.9.2/
Validation0/work"]
FeynmanGauge = True
WriteCHOutput[LDarkMatterValidation, Output -> "models"];
```

## A.4 Executing the model

### A.4.1 YAML file for cosmic microwave background constraints

```
Parameters:

  LCDM:
    omega_b: 0.022
```

```

    omega_cdm: 0.1188
    H0: 70.0
    tau_reio: 0.0544
    T_cmb: 2.72548

PowerLaw_ps:
  ln10A_s: 3.044
  n_s: 0.9649
  r: 0
  N_pivot: 55

StandardModel_SLHA2: !import include/
  StandardModel_SLHA2_Planckbaseline.yaml

AnnihilatingDM_Thesis:
  mass_DM:
    range: [1e-2,1e2]
    prior_type: log
  mass_med:
    range: [1e-2,1e2]
    prior_type: log
  lambda_DM: 1
  lambda_med_ferm: 1
  lambda_med: 1
  version: 1

cosmo_nuisance_Planck_lite:
  A_planck: 1

Printer:

  printer: hdf5
  options:

    output_file: "Thesis_data_CMB.hdf5"
    group: "/AnnihilatingDM_Thesis"
    delete_file_on_restart: true

Scanner:

  use_scanner: de

  de:
    plugin: diver
    like: LogLike
    NP: 10000
    convthresh: 1e-3

ObsLikes:

- purpose:      LogLike
  capability:    Planck_nuisance_prior_loglike

- purpose:      LogLike
  capability:    Planck_lowl_loglike

```

```

    function:      function_Planck_lowl_TTEE_2018_loglike

- purpose:      LogLike
  capability:    Planck_highl_loglike
  function:      function_Planck_highl_TTEEE_lite_2018_loglike

- purpose:      Observable
  capability:    capability_for_sigmapv
  function:      function_sigmapv #Save evaluated cross section

- purpose:      Observable
  capability:    capability_for_omega
  function:      function_oh2 #Save evaluated cross relic density

Rules:

- capability:    DarkAges_1_2_0_init
  options:
    f_eff_mode:  false      # Calculate the single f_eff(z) rather
                        than the full f_c(z) table? By default f_c(z) is
                        calculated
    print_table: false      # Print the table to stdout. Useful for
                        debugging
    z_max: 1.e7             # Constant continuation of efficiency
                        table up to a given redshift. (f(z) = const. for 2.7e3 < z
                        < z_max)

- capability:    classy_MPLike_input
  function:      set_classy_input_with_MPLike
  module:        CosmoBit

- capability:    parameter_dict_for_MPLike
  function:      pass_empty_parameter_dict_for_MPLike

- capability:    multimode_input_parameters
  function:      set_multimode_inputs
  options:
    k_pivot: 0.002
    dlnk: 0.4
    numsteps: 200
    k_min: 1e-7
    k_max: 1e6

- capability:    classy_primordial_input
  function:      set_classy_parameters_parametrised_ps

Logger:

redirection:
[Debug]          : "debug.log"
[Default]         : "default.log"
[CosmoBit]        : "CosmoBit.log"
[Scanner]         : "Scanner.log"

KeyValues:

```

```

debug: false

default_output_path: "${TMPDIR}/Thesis/"

likelihood:
  model_invalid_for_lnlike_below: -1e30

```

#### A.4.2 YAML file for relic density constraints

```

Parameters:

  AnnihilatingDM_Thesis:
    mass_DM:
      range: [1e-2,1e2]
      prior_type: log
    mass_med:
      range: [1e-2,1e2]
      prior_type: log
    lambda_DM: 1
    lambda_med_ferm: 1
    lambda_med: 1
    version: 2

Printer:

  printer: hdf5
  options:

    output_file: "Thesis_data_RD.hdf5"
    group: "/AnnihilatingDM_Thesis"
    delete_file_on_restart: true

Scanner:

  use_scanner: de

  de:
    plugin: diver
    like: LogLike
    NP: 10000
    convthresh: 1e-3

ObsLikes:

- purpose:      LogLike
  capability:    lnL_oh2
  function:      lnL_oh2_Simple

- purpose:      Observable
  capability:    capability_for_sigwav
  function:      function_sigwav #Save evaluated cross section

- purpose:      Observable
  capability:    capability_for_omega
  function:      function_oh2 #Save evaluated relic density

```

Rules:

- capability: lnL\_oh2  
function: lnL\_oh2\_Simple  
dependencies:
  - capability: RD\_oh2  
function: RD\_oh2\_Thesis  
module: DarkBit
- capability: DarkAges\_1\_2\_0\_init  
options:
  - f\_eff\_mode: false # Calculate the single f\_eff(z) rather than the full f\_c(z) table? By default f\_c(z) is calculated
  - print\_table: false # Print the table to stdout. Useful for debugging
  - z\_max: 1.e7 # Constant continuation of efficiency table up to a given redshift. (f(z) = const. for 2.7e3 < z < z\_max)
- capability: classy\_MPLike\_input  
function: set\_classy\_input\_with\_MPLike  
module: CosmoBit
- capability: parameter\_dict\_for\_MPLike  
function: pass\_empty\_parameter\_dict\_for\_MPLike
- capability: multimode\_input\_parameters  
function: set\_multimode\_inputs  
options:
  - k\_pivot: 0.002
  - dlnk: 0.4
  - numsteps: 200
  - k\_min: 1e-7
  - k\_max: 1e6
- capability: classy\_primordial\_input  
function: set\_classy\_parameters\_parametrised\_ps

Logger:

```
redirection:
[Debug]      : "debug.log"
[Default]    : "default.log"
[CosmoBit]   : "CosmoBit.log"
[Scanner]    : "Scanner.log"
```

KeyValues:

```
debug: true

default_output_path: "${TMPDIR}/RD/"

likelihood:
  model_invalid_for_lnlike_below: -1e30
```

# B

## Additional figures

### B.1 Relic density

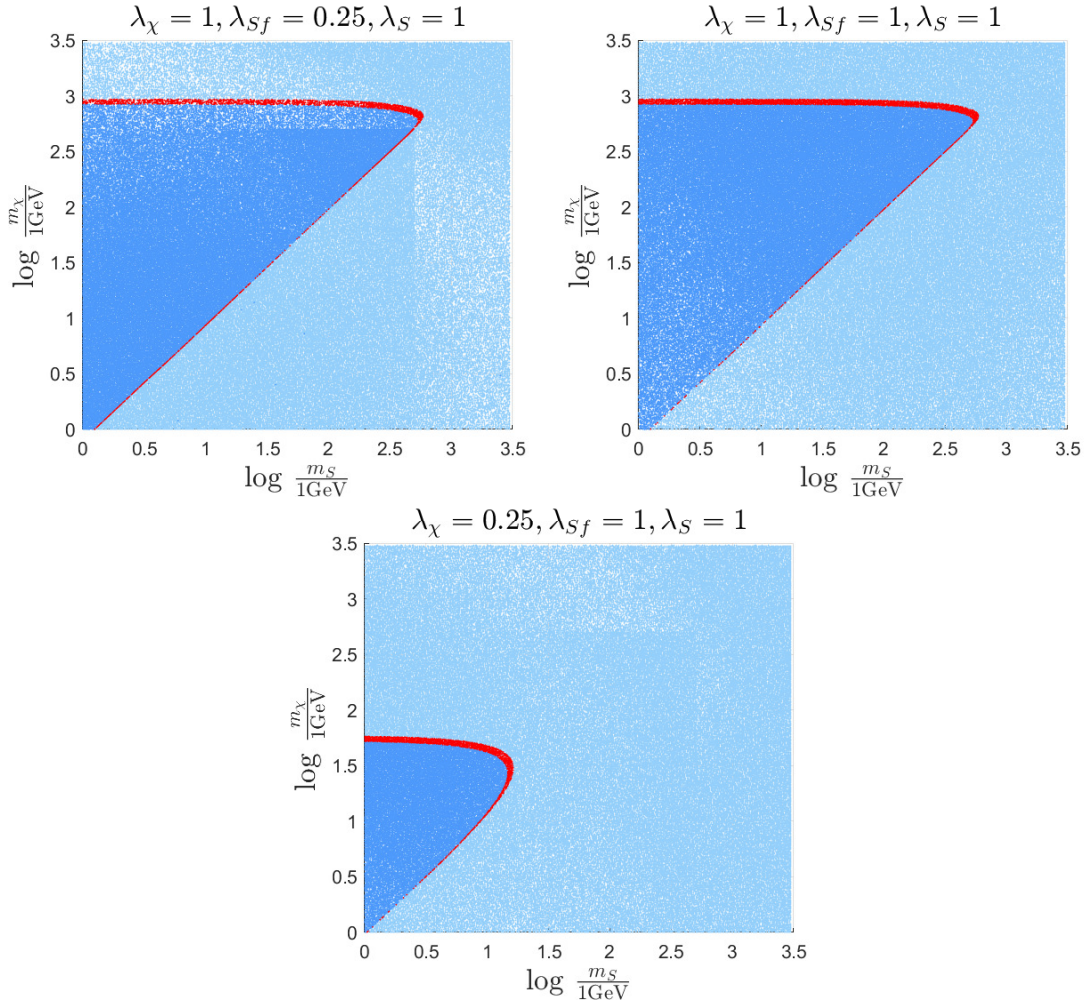


**Figure B.1:** Same as fig. 5.2, but for mass ranges  $m_\chi, m_S \in (1, 3 \cdot 10^3)$  GeV. In addition the region in parameter space where the evaluated relic density is smaller than the observed is highlighted in a darker shade of blue, while the region where the evaluated relic density is larger than the observed value is illustrated in lighter shade of blue.

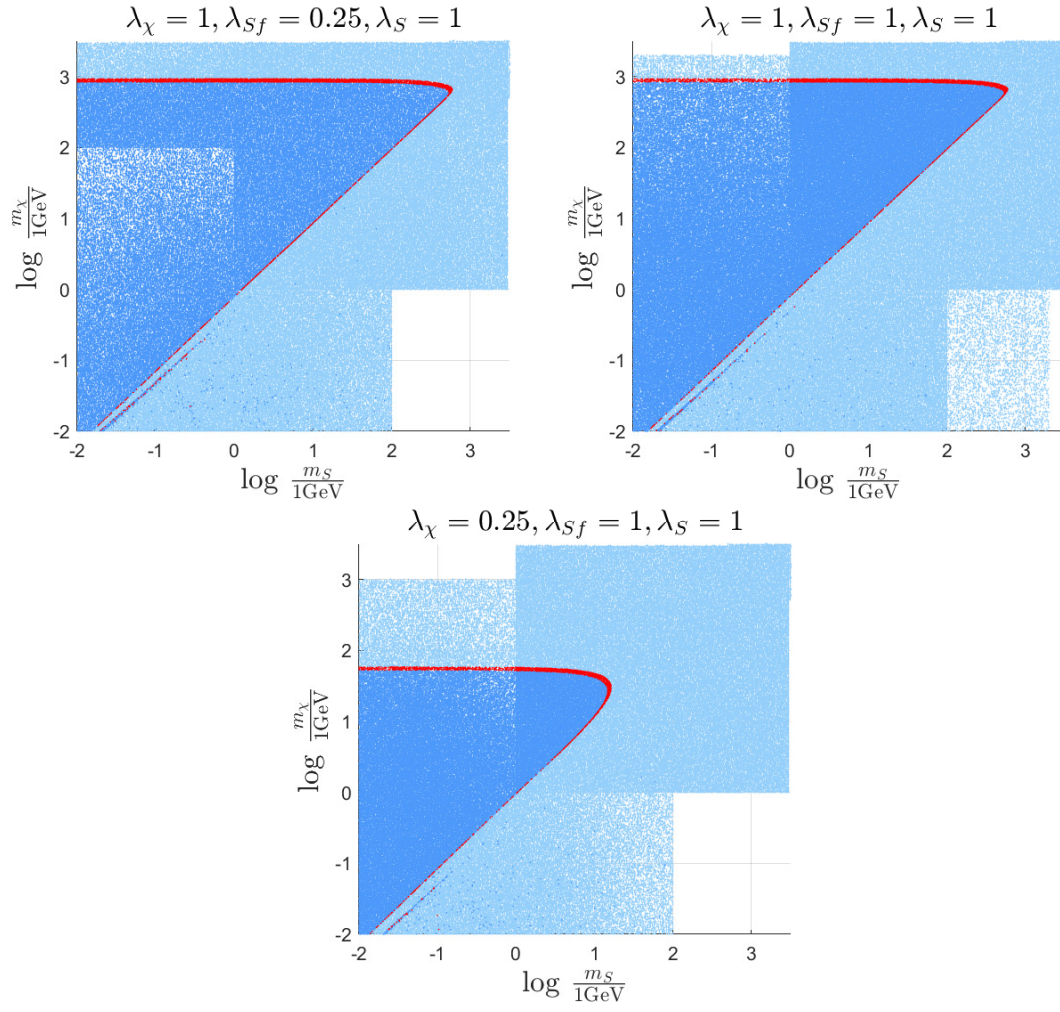


**Figure B.2:** Same as fig. B.1, but for mass ranges  $m_\chi, m_S \in (10^{-2}, 3 \cdot 10^3)$  GeV.



## B.2 Cosmic microwave background

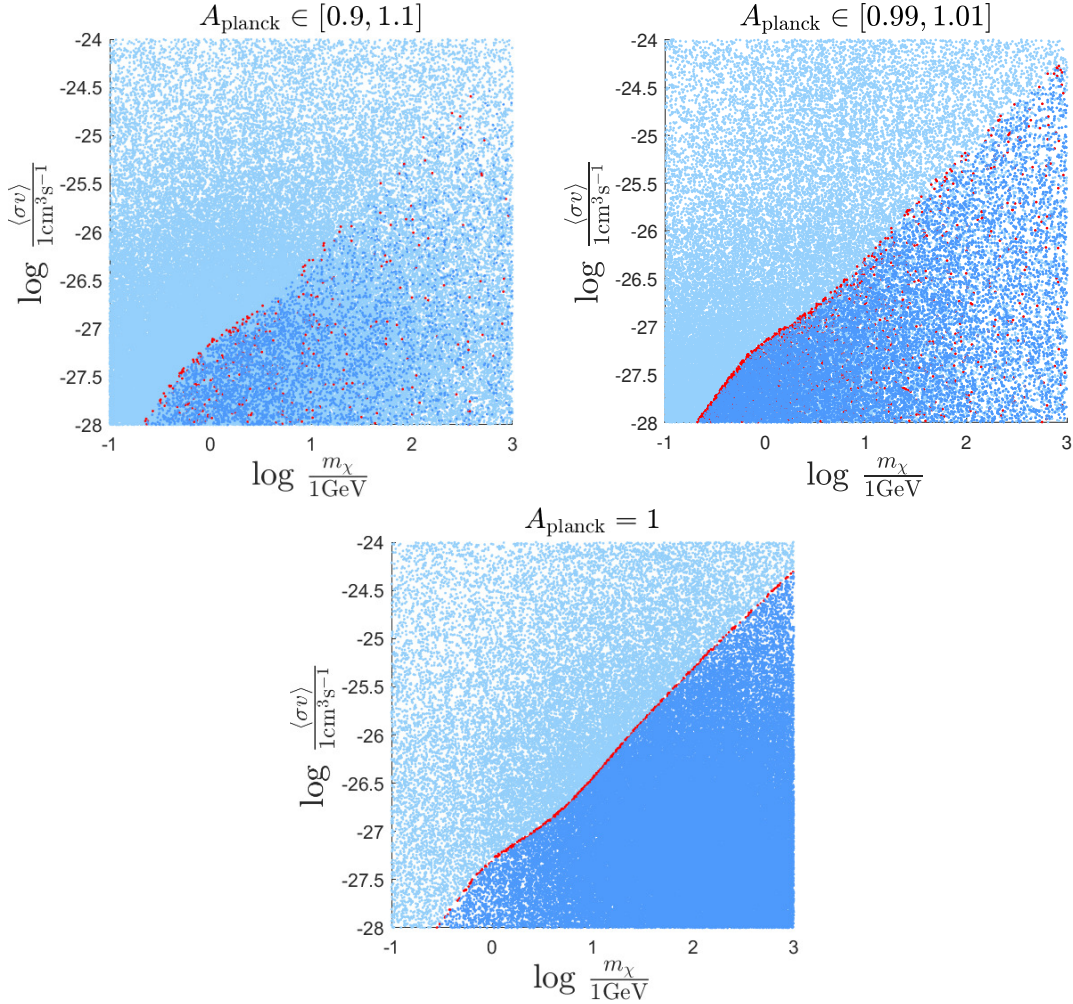


**Figure B.3:** Likelihood plots in the  $(m_\chi, \langle\sigma v\rangle)$  parameter space for different ranges of the nuisance parameter  $A_{\text{Planck}}$ . In the upper left plot the default range was used, i.e.,  $A_{\text{Planck}} \in [0.9, 1, 1]$ . In the upper right plot a more restricted range was used,  $A_{\text{Planck}} \in [0.99, 1, 01]$ . In the bottom plot the value was fixed to  $A_{\text{Planck}} = 1$ . The points illustrated in a lighter shade of blue make up the excluded region with 95% confidence as evaluated as described in section 5.4.

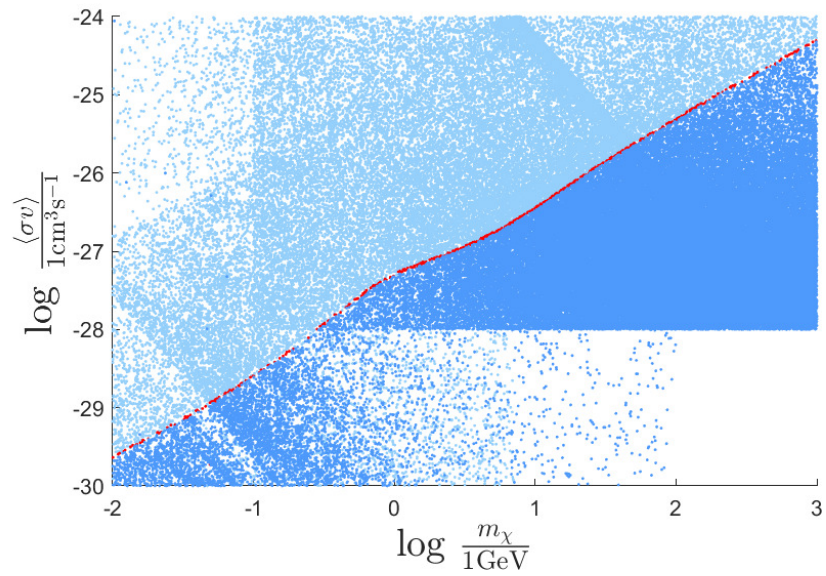


**Figure B.4:** Constraints on the parameter space  $(m_\chi, \langle\sigma v\rangle)$  when studying the CMB power spectrum. The points illustrated in a lighter shade of blue make up the excluded region with 95% confidence as evaluated as described in section 5.4. These results should be compared to fig. 9 in [2].

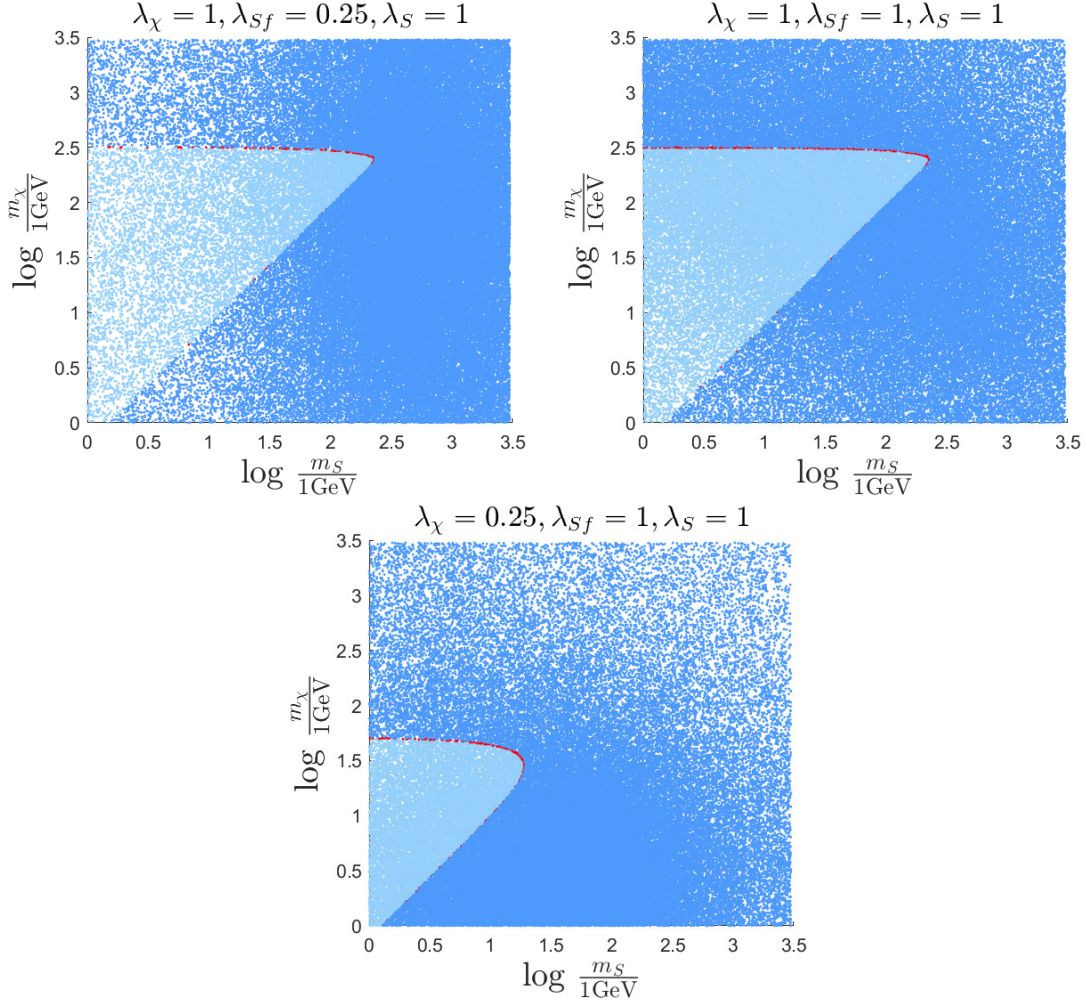


**Figure B.5:** Likelihood plots in the  $(m_\chi, m_S)$  parameter space in the ranges  $m_\chi, m_S \in [1, 3 \cdot 10^3]$  GeV for different sets of coupling strengths when comparing to CMB data. The sets of coupling strengths used were  $(\lambda_\chi, \lambda_{Sf}, \lambda_S) = (1, 0.25, 1), (1, 1, 1)$  and  $(0.25, 1, 1)$  for the upper left, upper right and bottom plot respectively. The points illustrated in a lighter shade of blue make up the excluded region with 95% confidence as evaluated as described in section 5.4.

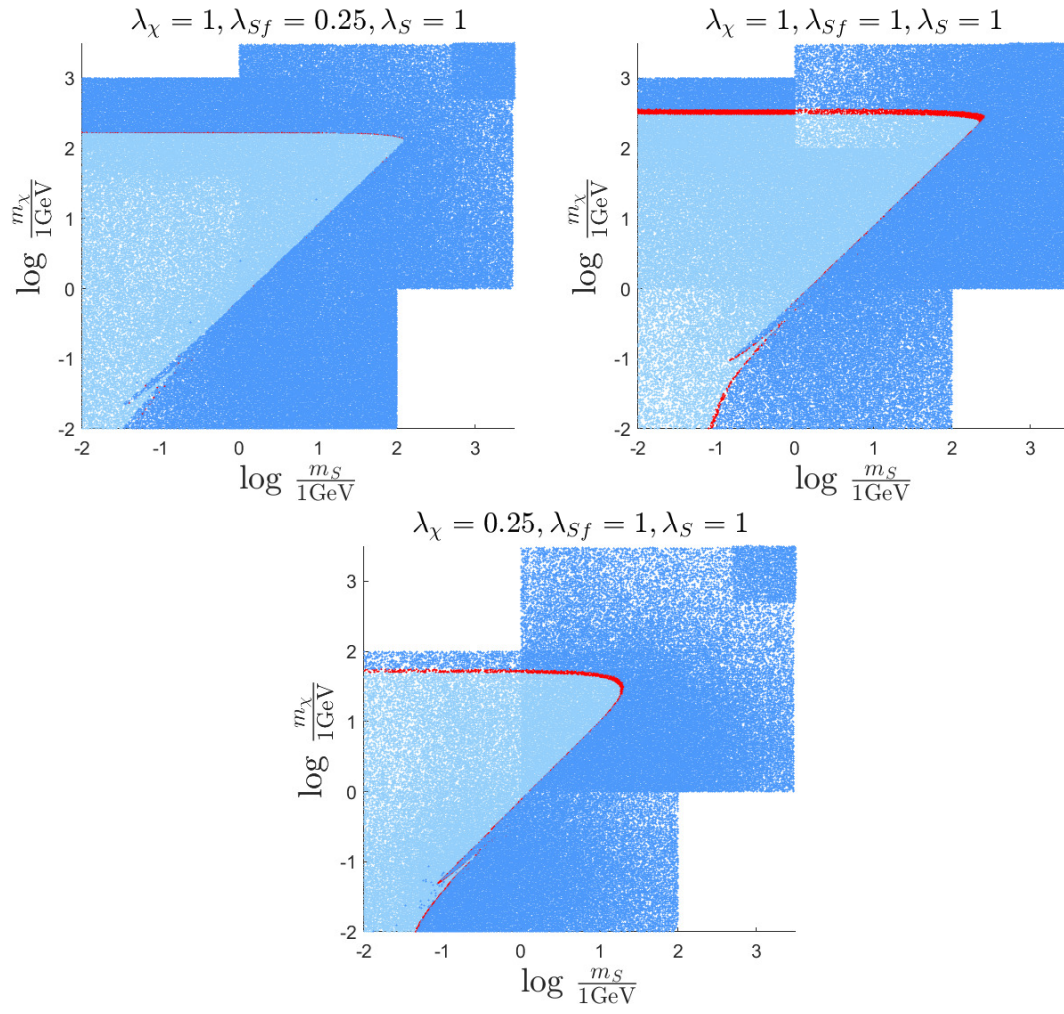


**Figure B.6:** Same as fig. B.5 but with additional regions included.



### B.3 Combined constraints

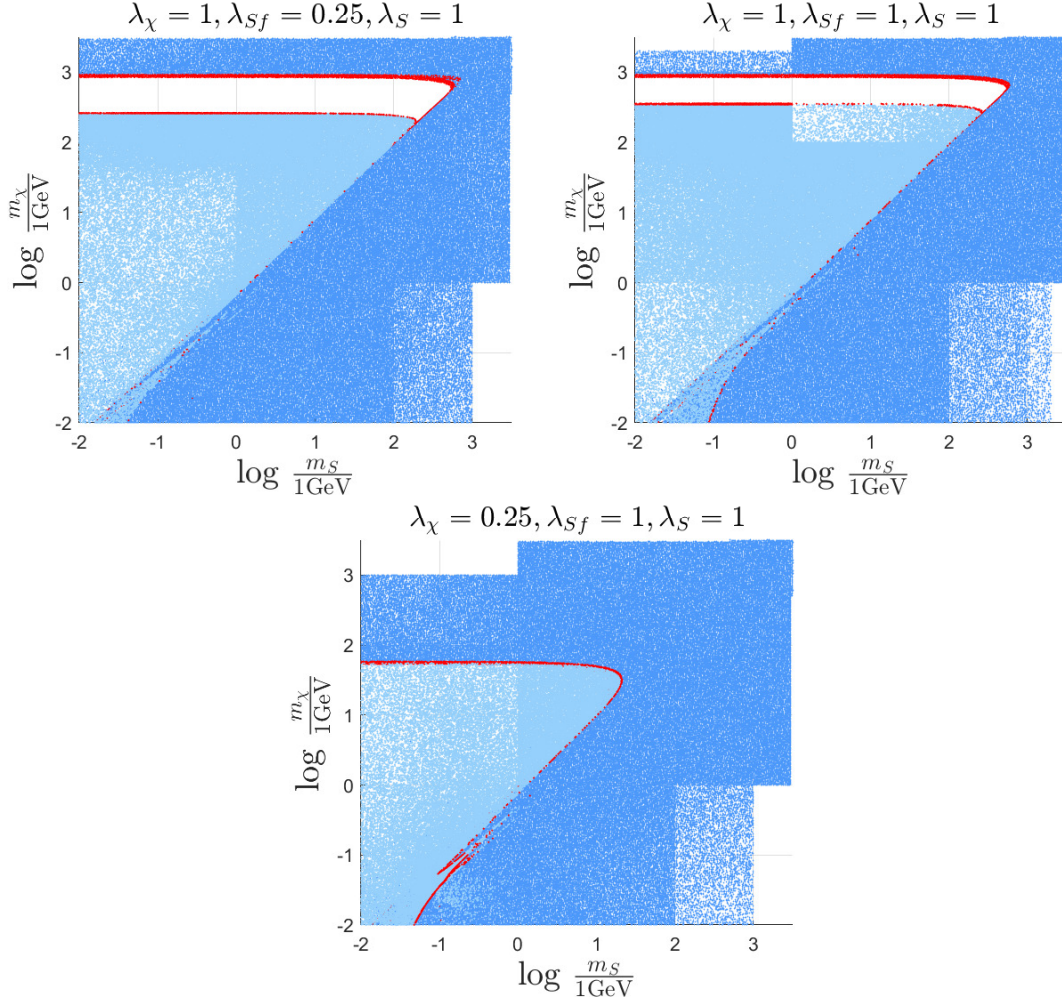


**Figure B.7:** The combined excluded regions from both relic density and CMB data. The regions that are excluded for yielding DM relic density that is too large is illustrated in dark blue, while the regions that are excluded from CMB data is illustrated in light blue. The white regions are not excluded.

DEPARTMENT OF SOME SUBJECT OR TECHNOLOGY  
CHALMERS UNIVERSITY OF TECHNOLOGY  
Gothenburg, Sweden  
[www.chalmers.se](http://www.chalmers.se)



**CHALMERS**  
UNIVERSITY OF TECHNOLOGY